

Vesicular apparatus, including functional calcium channels, are present in developing rodent optic nerve axons and are required for normal node of Ranvier formation

James J. P. Alix¹, Annette C. Dolphin² and Robert Fern¹

¹Department of Cell Physiology & Pharmacology, University of Leicester, Leicester, UK

²Department of Pharmacology, University College London, London, UK

P/Q-type calcium channels are known to form clusters at the presynaptic membrane where they mediate calcium influx, triggering vesicle fusion. We now report functional P/Q channel clusters in the axolemma of developing central axons that are also associated with sites of vesicle fusion. These channels were activated by axonal action potentials and the resulting calcium influx is well suited to mediate formation of a synaptic style SNARE complex involving SNAP-25, that we show to be located on the axolemma. Vesicular elements within axons were found to be the sole repository of vesicular glutamate in developing white matter. The axonal vesicular elements expressed the glutamate transporter V-ATPase, which is responsible for vesicular glutamate loading. The P/Q channel α_{1A} subunit was found to be present within the axolemma at early nodes of Ranvier and deleterious mutations of the α_{1A} subunit, or an associated $\alpha_2\delta$ -2 subunit, disrupted the localization of nodal proteins such as voltage-gated sodium channels, β IV spectrin and CASPR-1. This was associated with the presence of malformed nodes of Ranvier characterized by an accumulation of axoplasmic vesicles under the nodal membrane. The data are consistent with the presence of a vesicular signalling pathway between axons and glial cells that is essential for proper development of the node of Ranvier.

(Resubmitted 11 April 2008; accepted after revision 27 June 2008; first published online 3 July 2008)

Corresponding author R. Fern: Department of Cell Physiology & Pharmacology, University of Leicester, PO Box 138, University Road, Leicester LE1 9HN, UK. Email: rf34@le.ac.uk

Myelinated axons are responsible for the rapid transmission of action potentials around the nervous system. A high conduction velocity of axons is achieved by restricting the generation of action potentials to nodes of Ranvier that are spaced at regular intervals along the axon, separated by stretches of insulating myelin laid down by oligodendrocytes. Formation of the node of Ranvier involves clustering of the Na^+ channels responsible for action potential generation at node sites as myelin is deposited along the internodal region (Rasband & Shrager, 2000; Girault & Peles, 2002; Salzer, 2003). Na^+ channel clustering is preceded by the clustering of several components of a Na^+ channel–cytoskeletal complex, including ankyrin G and β IV spectrin (Lambert *et al.* 1997; Rasband *et al.* 1999; Jenkins & Bennett, 2002). Mediators of axon–glial interaction such as CASPR-1 also form clusters at early node sites before Na^+ channels start to aggregate (Rasband *et al.* 1999), and the whole process is apparently dependent upon a soluble factor released

by oligodendrocytes (Kaplan *et al.* 1997). It is currently unclear what determines where nodes will form or how the aggregation of the components of the node is controlled.

Intracellular Ca^{2+} ($[\text{Ca}^{2+}]_i$) regulates the outgrowth of axons (Henley & Poo, 2004; Conklin *et al.* 2005) and the formation of neuronal structures such as dendrites (Konur & Ghosh, 2005). Localized $[\text{Ca}^{2+}]_i$ changes could also potentially coordinate the development of the node of Ranvier. Local Ca^{2+} changes could be produced by focal expression of voltage-gated Ca^{2+} channels along axons (Mackenzie *et al.* 1996; Forti *et al.* 2000). Ca^{2+} channels are heteromeric membrane proteins that play an important role in the regulation of numerous cellular processes and are classified according to their electrophysiological and pharmacological properties (L-, N-, P/Q-, R- and T-type). Each Ca^{2+} channel type is composed of a pore-forming α_1 subunit and a number of accessory subunits. It is the α_1 subunit that distinguishes Ca^{2+} channel subtype and there are currently 10 α_1 subunit genes known (Catterall, 2000). The α_1 subunit contains the elements responsible for voltage-dependent gating of the channels, which may be modulated by accessory subunits.

This paper has online supplemental material.

While the axons of mammalian neurons possess several proteins involved in Ca^{2+} homeostasis, evidence for the expression of functional Ca^{2+} channels on the axolemma has been slow to reveal itself. Past reports in the literature have suggested that axonal Ca^{2+} channels may, under physiological circumstances, play a part in the regulation of action potential frequency and the non-vesicular release of neurotransmitter substances at *en passant* synapses (Callewaert *et al.* 1996; Forti *et al.* 2000). More recently, vesicular release of glutamate has been demonstrated in both the corpus callosum and immature rat optic nerve (Kukley *et al.* 2007; Ziskin *et al.* 2007). Both studies independently reported activity-dependent activation of AMPA receptors on NG2(+) cells following vesicular glutamate release, predominantly from unmyelinated axons. Kukley *et al.* (2007) provided evidence that this synapse-like form of axon–glia communication was initiated by rapid Ca^{2+} signalling within Ca^{2+} microdomains in axons. Here we provide evidence that clustered axonal Ca^{2+} channels play a significant role in action potential conduction in neonatal central axons and make a pivotal contribution to the development of the node of Ranvier. The Ca^{2+} channels involved are largely of the synaptic P/Q-type and we provide additional evidence that they are involved in co-ordinating the fusion of vesicular elements from the axoplasm to the axolemma of developing axons.

Methods

Ethical approval

All animal procedures were approved by local ethical review and conformed to UK Home Office regulations. Animals were killed by vertebral dislocation or CO_2 inhalation depending upon age.

General

Optic nerves were dissected from Lister-hooded rats and perfused with artificial cerebrospinal fluid (aCSF) of composition (mM): NaCl, 126; KCl, 3; NaH_2PO_4 , 2; MgSO_4 , 2; CaCl_2 , 2; NaHCO_3 , 26; glucose, 10; pH, 7.45, bubbled with 5% CO_2 –95% O_2 and maintained at 37°C. Bicarbonate, sulphates and phosphates were omitted from the high divalent cation solutions used to evoke divalent cation action potentials (osmolarity maintained with sucrose). These solutions contained 10 mM Hepes and were buffered to pH 7.45. Data are mean \pm S.E.M., significance determined by ANOVA with Tukey's post test. Unless otherwise stated all chemicals were purchased from Sigma (UK).

Electrophysiology

Extracellular compound action potentials were evoked and recorded with suction electrodes. Peak-to-peak

amplitude was used to assess changes in the number of unitary action potentials in the neonate since action potential area cannot be applied reliably to recordings from neonatal nerves. This is due to the large stimulus artifact produced by the longer stimulus times that are required to elicit a full neonatal compound action potential (Foster *et al.* 1982; Fern *et al.* 1998).

Nerves were maintained in an interface perfusion chamber (Medical Systems, Greenvale, New York, NY, USA), and continuously oxygenated with 5% CO_2 –95% O_2 . Individual nerves were electrically stimulated via a suction electrode at one end using square-wave constant current pulses of 150–600 μs (< P15) or 50 μs (> P15) duration (Iso stim A320, WPI), and compound action potentials recorded via a second suction electrode at the other end (Cyber Amp 320, Axon Instruments). The recorded signal was subtracted from a parallel differential electrode, filtered (low pass: 800–10000 Hz, depending upon animal age), digitized (25000 Hz: 1401 mini, Cambridge Electronic Design) and displayed on a PC running Signal software (Cambridge Electronic Design) with positive (relative to the subtraction electrode) going up. Lower filter settings were used for neonatal nerves to prevent distortion of the wave form due to the slow time-course of the wave compared to those recorded from adult nerves.

Immuno-histochemistry

Optic nerves were dissected into 0.1 M PBS and fixed in 4% paraformaldehyde for 30 min. The optic nerves were subsequently incubated in 0.1 M PBS plus 20% sucrose w/v for 5 min prior to freeze-sectioning (20 μm sections) and subsequent blocking for 60 min in 0.1 M PBS, 10% fetal goat serum plus 0.5% Triton-X 100. Sections were then incubated in this solution plus primary antibody at 4°C overnight. Primary antibodies included: polyclonal α_{1A} (Alomone; 1:200), α_{1B} , α_{1C} , α_{1D} (Sigma; 1:200), and affinity-purified $\alpha_2\delta$ -2 (Brodbeck *et al.* 2002; 1:200). In double-staining experiments, second primary incubations were at room temperature for 2 h: monoclonal antipan-Na⁺ channel (Sigma; 1:200), anti-neurofilament-70 (NF-70) or anti-neurofilament-200 (NF-200) (Chemicon; 1:100 and 1:200, respectively), anti-GFAP (Glial Fibrillary Acidic Protein) (Sigma; 1:500), anti-CNPase (2', 3'-cyclic nucleotide 3'-phosphodiesterase) (Sigma; 1:100), or anti-CASPR-1 (1:1000) were used. The axonal markers NF-70 and NF-200 tend to label small diameter and larger diameter axons, respectively (Sanchez *et al.* 2000). Appropriate Alexa-conjugated secondary antibodies (Cambridge Bioscience; 1:1000) were subsequently applied for 1 h and sections examined by scanning confocal microscopy using an Olympus FV300 Fluoview confocal image system.

Images were analysed using either Metamorph (Universal Imaging Corporation) or Image J (NIH). Images of Na^+ and Ca^{2+} channel clusters were analysed using Image J using the Cell Counter plug-in. Random single optical section fields of view (FOV) were taken from a minimum of three nerves with no more than three FOVs being taken from a single nerve, resulting in a sample number of at least nine. When such analysis was done using two or more different ages, or with either leaner or ducky mice and their respective controls, the individual performing the analysis (J.J.P.A.) was blinded to the images in order to avoid any potential bias. The degree to which Ca^{2+} channel clusters co-localized with cell-specific markers was assessed by counting the number of times the Ca^{2+} channel clusters either did, or did not, completely overlap with the marker within a field of view. The degree of co-localization was then reported as a percentage of the total number of Ca^{2+} channel clusters within the FOV. The degree of association of Ca^{2+} channel clusters with the paranodal marker CASPR-1 was assessed by observing the number of times clusters within a FOV either were co-localized (defined as complete overlap) or were immediately adjacent (defined as touching or partial overlap) to CASPR-1 immunoreactivity. The degree of association between these two markers is taken to be the degree of adjacent and co-localized markers combined. Finally, neurofilament intensity was calculated using Metamorph software.

Electron microscopy

Optic nerves from P23–P25 mice and P10 rats were post-fixed in 3% glutaraldehyde in Sorenson's phosphate buffer. Nerves from Leaner mice were obtained from Jackson Laboratories (MA, USA) and were fixed according to our instruction. Nerves were then post-fixed with 2% osmium tetroxide and dehydrated prior to infiltration in epoxy. Sections were counterstained with uranyl acetate and lead citrate and examined with a Jeol 100CX electron microscope (see Thomas *et al.* (2004) for further details). For post-embedding immuno-labelling, primary antibody was applied to the sections overnight. Antibodies raised against: α_{1A} (Alomone; 1:200), SNAP-25 (Sigma; 1:50), V-ATPase (Santa Cruz Biochem; 1:50), glutamate (Chemicon International; 1:25–1:50) were used and appropriate 20–30 nm gold particle secondary antibodies were applied following washing. Controls involved omitting primary antibodies, which resulted in zero staining. The anti-SNAP-25 antibody was used at the same concentration by Kolk *et al.* (2000), who demonstrated a synaptic pattern of staining in CNS grey matter, in addition to a lower level of axonal staining. The anti-glutamate antibody has been described in prior publications (e.g. Back *et al.* 2006), where a range of controls are described.

Results

Functional voltage-gated calcium channels on neonatal central axons

To probe for the presence of functional Ca^{2+} channels on developing axons we determined whether the axons can support a divalent cation-mediated compound action potential (DCAP) (Fatt & Ginsborg, 1958). Na^+ channels were blocked by perfusion with zero- Na^+ aCSF + 1 μM TTX, abolishing the normal action potential (Fig. 1A–C). Subsequently increasing the extracellular divalent cation concentration to 40 mM of both Ca^{2+} and Ba^{2+} (total divalent cation concentration = 80 mM) to potentiate current through Ca^{2+} channels produced an action potential from P2 to P12, but not at P22 (Fig. 1A–C). Between 10 and 20 min of perfusion with high concentrations of divalent cation solution was required before a DCAP appeared, consistent with the slow diffusion of the ions into the extracellular space (Fern & Harrison, 1988). The DCAP recorded from the neonatal optic nerve was similar to the Na^+ action potential in amplitude but was relatively slower conducting (0.1–0.3 m s^{-1} compared to 1–3 m s^{-1}). Slow action potential conduction will be partly due to differences in channel kinetics between Ca^{2+} channels and Na^+ channels and partly to the surface negative charge screening effects of the divalent ions. High concentrations of Ca^{2+} and Ba^{2+} will increase the screening of fixed negative charge on the extracellular surface of the axon, effectively raising the activation threshold of voltage-gated channels (Brismar & Frankenhaeuser, 1972; Hille, 1998). Removal of extracellular Na^+ will produce a degree of membrane depolarization that will partially counter this effect, while rapid depletion of axoplasmic Na^+ will block any effect of Na–Ca exchange (NCX) upon membrane potential or ion fluxes (Stys *et al.* 1992; Leppanen & Stys, 1997). Although relatively slow, the rate of DCAP conduction precludes the possibility that the potential is conducted down glial cells in the optic nerve as a form of spreading depression. Spreading depression propagates at three to four orders of magnitude more slowly than the DCAP (between 30 and 50 $\mu\text{m s}^{-1}$), travels only relatively short distances from a point stimulation ($\sim 500 \mu\text{m}$), lasts over four orders of magnitude longer ($\sim 100 \text{ s}$), and does not operate in central white matter (e.g. Peters *et al.* 2003; Fabricius *et al.* 2006; Smith *et al.* 2006). A contribution from divalent cations passing through TTX-resistant Na^+ channels can also be discounted since the Ca^{2+} permeability of Na^+ channels is low, high Ca^{2+} concentrations block Na^+ channels (Hille, 1998; Armstrong & Cota, 1999), and the TTX-insensitive Na^+ channels in the axons are not capable of supporting an action potential (TTX completely blocks the normal Na^+ action potential). Furthermore robust DCAPs were observed when Ba^{2+} alone was used as the charge carrier (see below), while Ba^{2+}

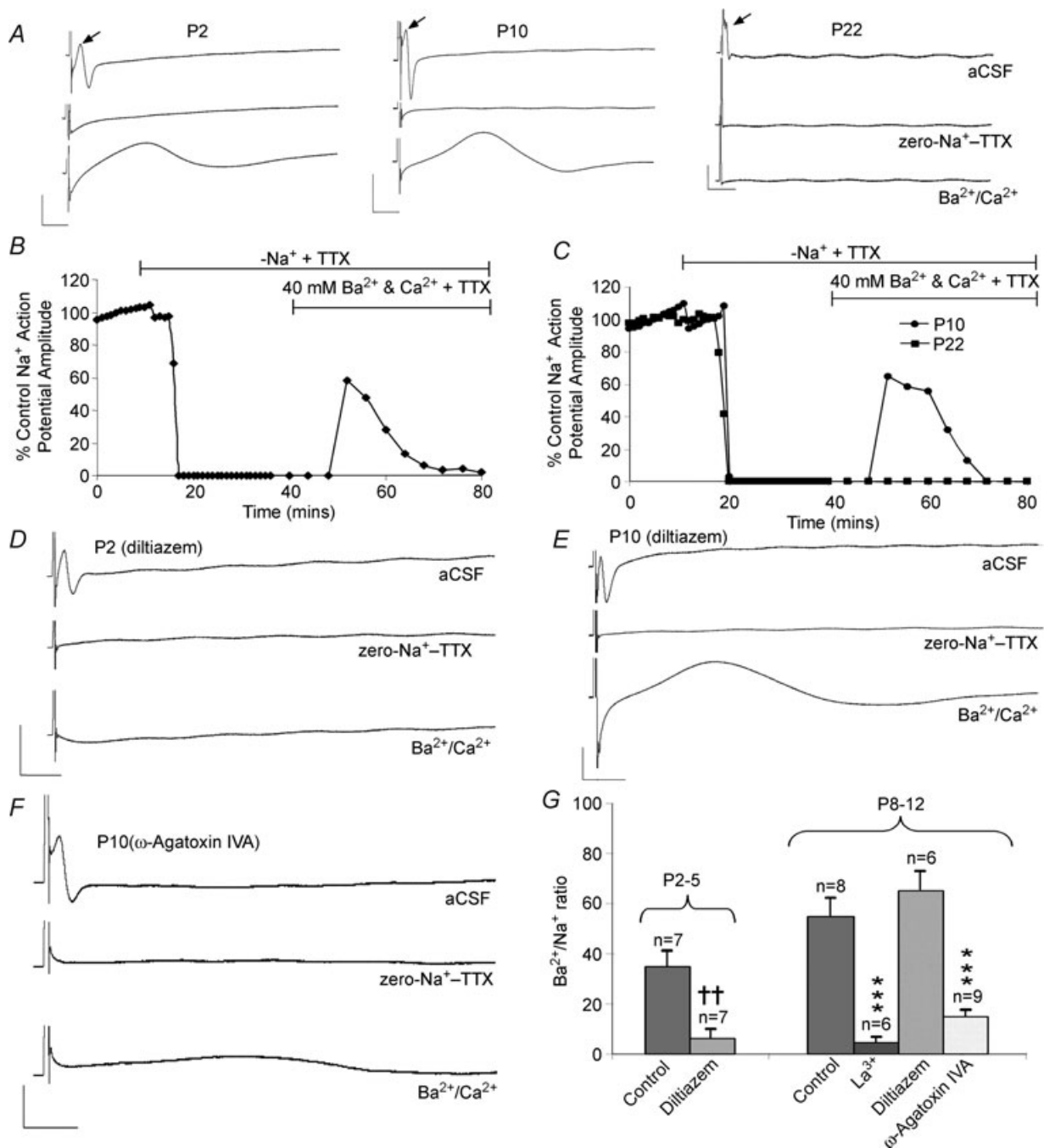


Figure 1. Divalent cation action potentials can be produced in neonatal rat optic nerve axons

A, compound action potentials recorded at three developmental ages. Top traces show the normal, fast-conducting, action potential (arrow), following the stimulus artefact). Middle traces show block of this action potential in zero-Na⁺-TTX (1 μM). Lower traces show a large amplitude, slow-conducting, action potential recorded in the presence of 40 mM of both Ba²⁺ and Ca²⁺ (still in zero-Na⁺-TTX). Note the absence of a divalent cation action potential at P22. B, action potential amplitude recorded at P2 versus time. Zero-Na⁺-TTX blocks the action potential after ~10 min and switching to Ba²⁺-Ca²⁺ produces a divalent cation action potential after 12 min that then declines slowly. C, similar plot of action potentials at P10 and P22. D, traces of normal action potential, block in zero-Na⁺-TTX and perfusion with Ba²⁺-Ca²⁺ (in zero-Na⁺-TTX) solution at P2 in the presence of the specific L-type blocker diltiazem (50 μM). No divalent cation action potential is apparent. E, similar data at P10, showing large divalent cation action potential in diltiazem. F, experiment as above demonstrating a much reduced divalent cation action potential in the presence of ω-agatoxin IVA (100 nM). G, amplitude of the divalent cation action potential relative to normal action potential at various ages. The divalent cation action potential was blocked by diltiazem at P2–P5 but not at P8–P12. ω-Agatoxin IVA significantly blocked the divalent cation action potential at P8–P12, as did the non-selective calcium channel blocker La³⁺ (100 μM). Error bars are s.e.m., ****P* < 0.001 versus control P8–P12, ††*P* < 0.01 versus control P2–P5. Scale bars are 10 mV and 10 ms.

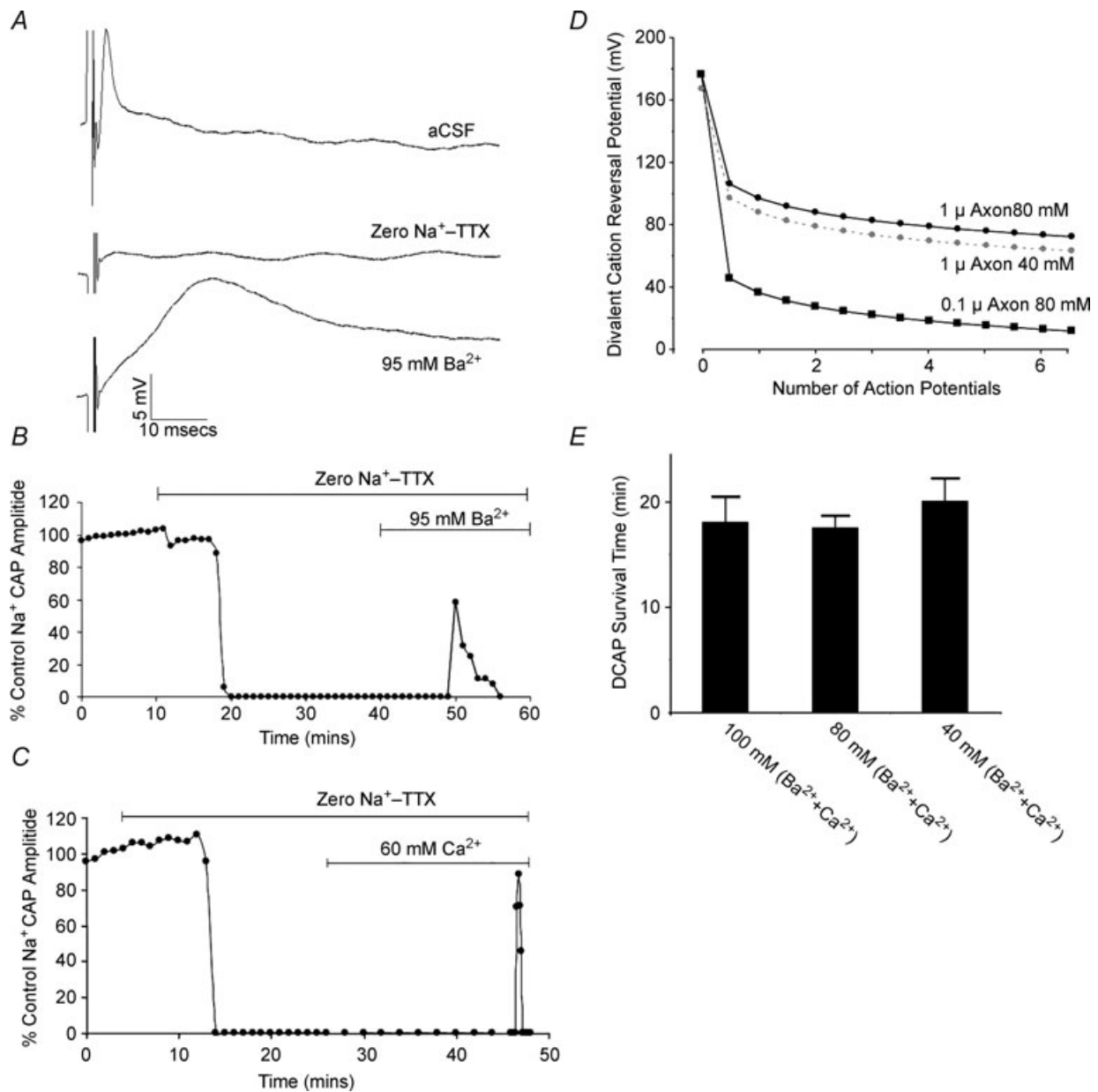


Figure 2. Features of the DCAP in P8–P12 rat optic nerve

A, high concentrations of a single divalent cation can produce a DCAP. Top, a normal compound action potential recorded in aCSF. Middle, block of this action potential in zero- Na^+ -TTX solution. Bottom, a large-amplitude, slow-conducting DCAP is recorded in the presence of 95 mM Ba^{2+} . B, action potential amplitude is plotted against time, demonstrating the decline in the DCAP over an ~10 min time course. C, a similar protocol showing the time-course of a DCAP recorded in 60 mM Ca^{2+} . Switching to zero- Na^+ -TTX solution produced block of the normal action potential and changing to 60 mM extracellular Ca^{2+} resulted in a short-lasting DCAP. D, the divalent cation reversal potential in axons calculated assuming a starting axoplasmic concentration of 100 nM, an extracellular divalent cation concentration of 90 mM, a resting membrane potential of -70 mV, a DCAP amplitude of 100 mV and a membrane capacitance of $1 \mu\text{F cm}^{-2}$. It is also assumed that there is no significant extrusion of divalent cations entering during the DCAP and that there is no influx into the axon when the axolemma is at rest. Given these assumptions, it is apparent that a small number of divalent cation action potentials have a dramatic effect upon the divalent cation reversal potential, in particular for the smaller diameter axons (0.1 μm , filled squares). Reducing the extracellular divalent cation concentration to 40 mM has minimal effect upon the time course of the collapse of the reversal potential (grey circles, plotted for a 1 μm axon). E, the time between the first appearance of a DCAP and its failure (survival time) in various high divalent cation conditions, showing that varying the total divalent cation concentration between 40 and 100 mM had no significant affect, as predicted in D.

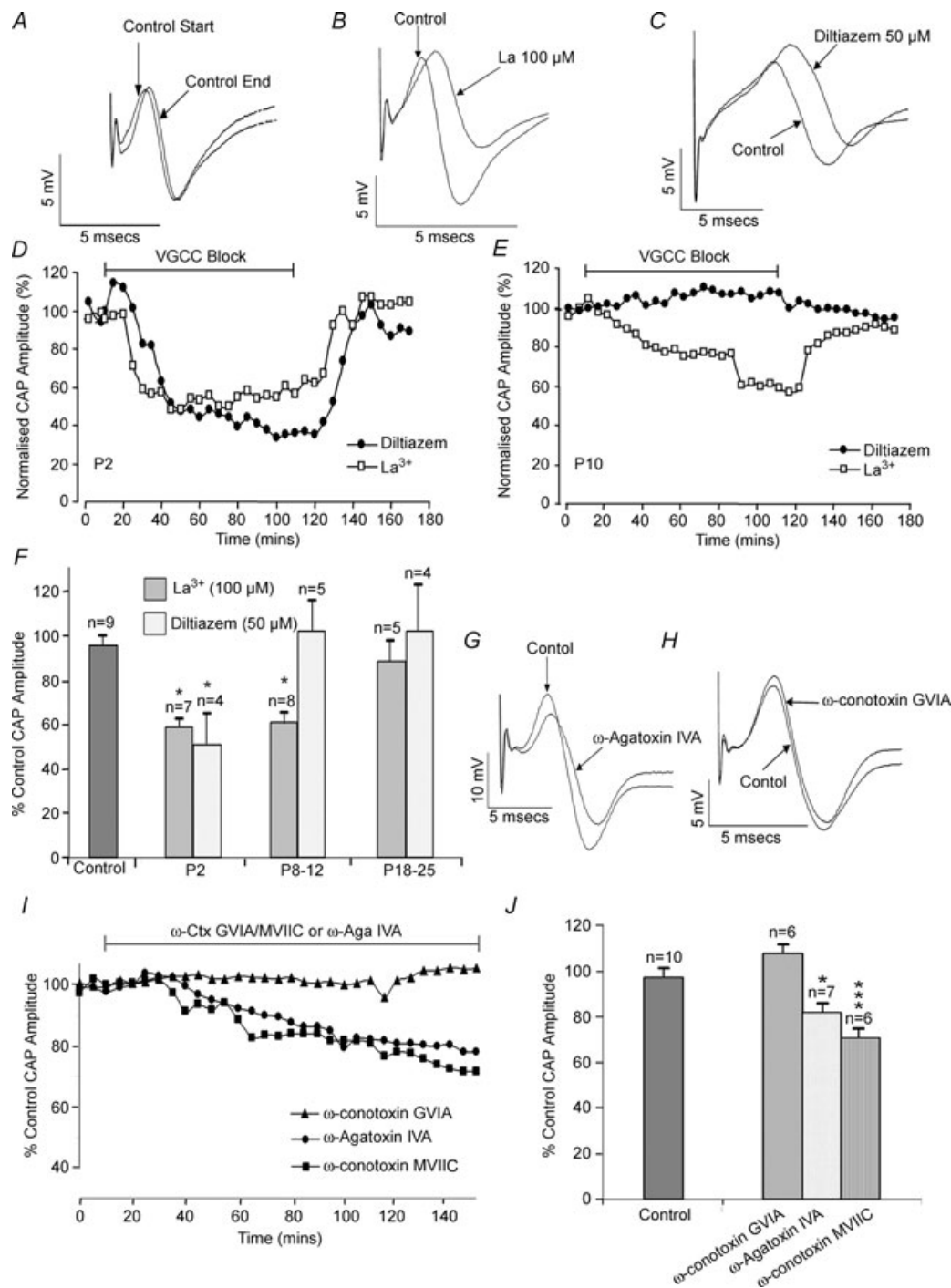


Figure 3. Ca²⁺ channels contribute to normal action potentials in developing axons

A, P12 control showing the compound action potential recorded at $T = 0$ min (control start) and $T = 150$ min (control end). *B*, non-selective Ca²⁺ channel block with La³⁺ reduced action potential amplitude at P12. *C*, block of L-type channels with diltiazem at P12 did not reduce action potential amplitude (slowing is evident). *D*, La³⁺ and diltiazem produced a similar, reversible, decline in the compound action potential at P2. *E*, La³⁺ but not diltiazem produced a reversible decline in the action potential at P10. *F*, summary showing the effect of La³⁺ and diltiazem upon compound action potential amplitude at different ages. *G*, block of P/Q-type channels with ω-agatoxin IVA (100 nM) reduced action potential amplitude at P12. *H*, block of N-type channels with ω-conotoxin GVIA (1 μM) had no significant affect at P12. *I*, time course of effect of ω-agatoxin IVA, ω-conotoxin GVIA and ω-conotoxin MVIC on action potential amplitude at P12. *J*, summary of the effects of ω-agatoxin IVA or ω-conotoxins upon action potential amplitude at P12. * $P < 0.05$, *** $P < 0.001$.

permeability through Na^+ channels is not measurable (Hille, 1998).

The Ca^{2+} channel-dependent nature of the DCAP was confirmed by application of selective Ca^{2+} channel blockers. The DCAP was blocked at P8–P12 by the broad-spectrum Ca^{2+} channel blocker La^{3+} ($100 \mu\text{M}$) (Fig. 1G). The selective L-type Ca^{2+} channel blocker diltiazem ($50 \mu\text{M}$) largely blocked the divalent cation action potential at P2–P5, but not at P8–P12 (Fig. 1D, E and G). The P8–P12 divalent cation action potential was largely blocked by the specific P/Q blocker ω -agatoxin IVA (Mintz *et al.* 1992) (100 nM) (Fig. 1F and G).

Perfusion with either divalent cation alone produced a DCAP (Fig. 2A–C). Once apparent, the DCAP declined over an ~ 20 min period, irrespective of whether it was Ba^{2+} or Ca^{2+} in the divalent cation solution (Fig. 2A–C), or both (Figs 1B, C and 2E). This effect may be due to the run-down of concentration gradients in the small diameter, small volume, neonatal rat optic nerve axons. Axons will lack Na-Ca exchange under these zero- Na^+ conditions (Stys *et al.* 1992; Leppanen & Stys, 1997), and divalent ions entering during an action potential are likely to remain in the axoplasm. The diameter of

axons in the P8–P12 rat optic nerve ranges between ~ 0.1 – $1.0 \mu\text{m}$ (Foster *et al.* 1982). The effect of a single 100 mV DCAP upon the divalent-cation reversal potential can be calculated using the equation $n = CV/2F$ where n is the number of divalent ions entering the axon during one action potential (in moles), C is the membrane capacitance ($1 \mu\text{F cm}^{-2}$), V is the action potential amplitude, and F is the Faraday constant. The DCAP amplitude is estimated at 100 mV since intra-axonal recording from optic nerve axons have never been achieved. The number of divalent cations within the resting axoplasm can be calculated from the cylinder volume and resting ion concentration, while the number of ions entering a given length of axon during a single action potential can be calculated from the voltage change across the membrane capacitance (Aidley, 1971). Assuming a resting axoplasmic divalent concentration of 100 nM , a single DCAP is predicted to result in a $20.2 \mu\text{M}$ rise in axoplasmic divalent cation concentration, producing a sharp decline in the divalent-cation reversal potential (Fig. 2D). The time-course of the DCAP was not significantly different in solutions with various divalent concentrations (Fig. 2E). However, the axoplasmic divalent cation concentration primarily

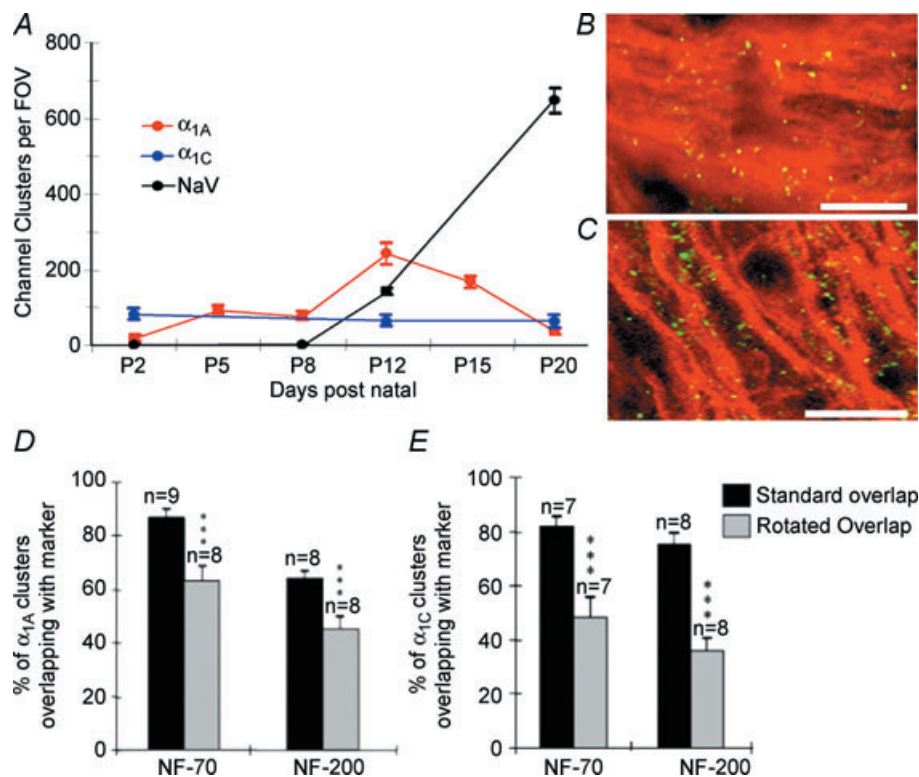
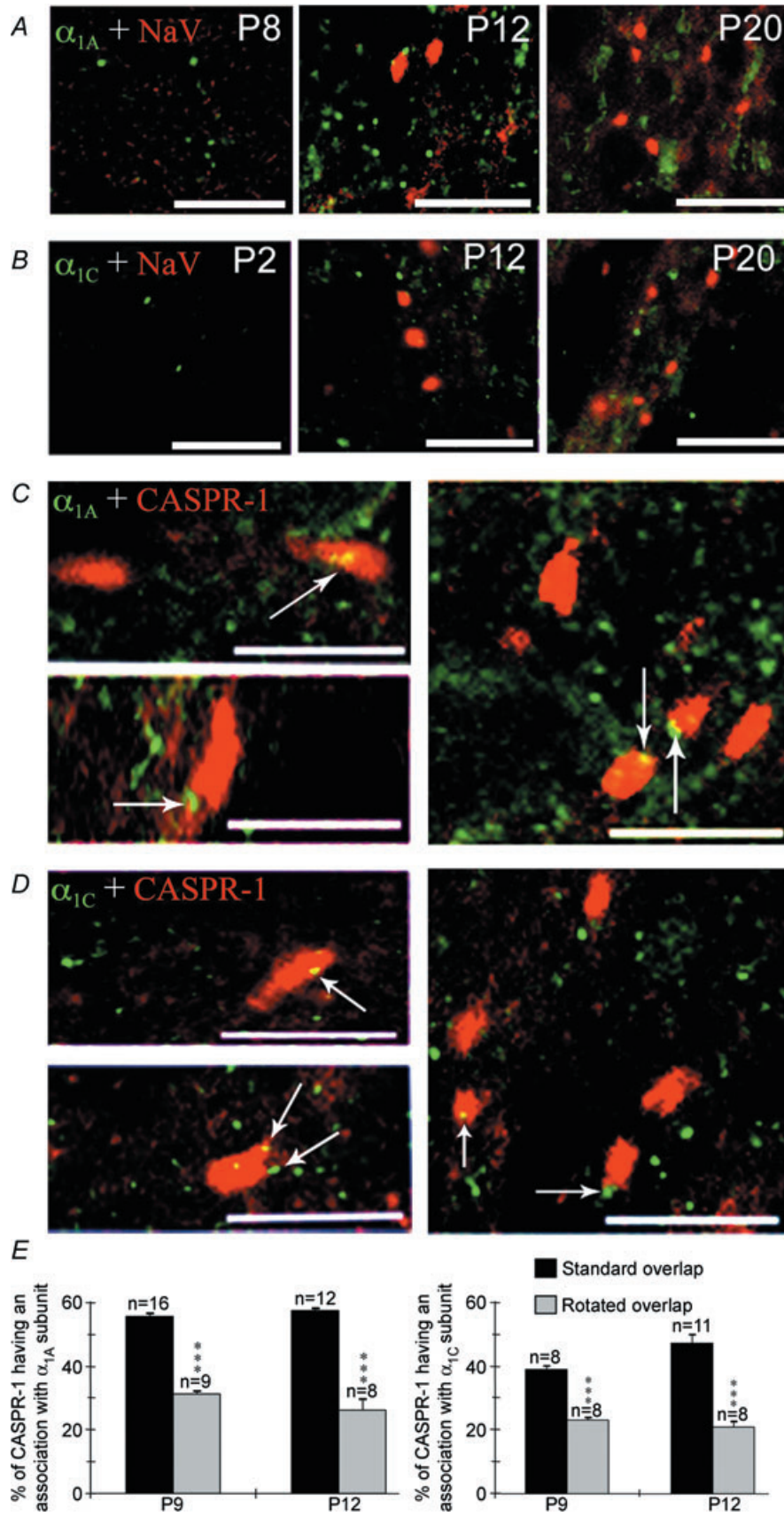


Figure 4. The evolution of ion channel clusters in optic nerve during development

A, the density of sodium channel (black), α_{1A} (red) and α_{1C} (blue) clusters during development. B, α_{1A} subunits (green) are clustered on NF-70(+) axons (red). C, few α_{1A} subunits (green) co-localized with CNPase(+) oligodendroglia (red). Some overlap is seen due to the close apposition of axons and myelinating oligodendrocyte processes. Scale bars, $10 \mu\text{m}$. D and E, rotating the NF-70 and NF-200 images by 90° significantly reduced the degree of co-localization, indicating a greater association than would be due to chance. A relatively high degree of association was still observed due to the ubiquitous nature of neurofilament staining. $***P < 0.001$.



determines the divalent cation reversal potential and these changes in extracellular divalent ion concentration are predicted to have only a small effect upon DCAP survival time (Fig. 2D). While these calculations are consistent with a collapse of divalent ion influx during repetitive stimulation, the associated rise in axoplasmic divalent-cation concentration may have other effects upon action potential conduction that might contribute to the relatively rapid conduction failure.

Calcium channel activation during action potential conduction

We examined the possibility that the calcium channels expressed by developing central axons might contribute to normal action potential conduction. Compound action potentials recorded from neonatal rat optic nerves were stable under control conditions of perfusion with normal aCSF (Fig. 3A), and exhibited a reversible fall in amplitude at P2–P5 (Fig. 3D and F) and P8–P12 (Fig. 3B, E and F) upon perfusion with the broad-spectrum calcium channel blocker La^{3+} ($100 \mu\text{M}$). This effect of La^{3+} was lost by P20 (Fig. 3F). The selective L-type calcium channel blocker diltiazem ($50 \mu\text{M}$) mimicked the effect of La^{3+} upon compound action potential amplitude at P2–P5 but not at later developmental stages (Fig. 3C–F). Diltiazem did slow action potential conduction at P8–P12, however (Fig. 3C), but had no comparable effect in P18–P25 optic nerves (data not shown). A similar partial conduction block was produced by nifedepine ($5 \mu\text{M}$) at P2, reducing amplitude by $44.5\% \pm 12.8\%$ ($n = 3$, data not shown). Nifedepine is not the L-type channel blocker of choice in this preparation, however (Fern *et al.* 1995). Block of P/Q-type channels with ω -agatoxin IVA (100 nM) at P8–P12 produced a significant fall in action potential amplitude, a result also obtained with the N- and P/Q-type blocker ω -conotoxin MVIIC ($1 \mu\text{M}$) (Fig. 3G, I and J). In contrast, specific block of N-type channels with ω -conotoxin GVIA ($1 \mu\text{M}$) had no effect (Fig. 3H–J). These data suggest that L-type calcium channels contribute to normal action potential conduction at P2–P5 (prior to the appearance of compact myelin in this preparation), that P/Q-type channels have a similar effect at P10 (when myelination is getting

underway), and that no significant contribution to action potential amplitude from calcium channels is apparent at P18–P25.

Synaptic-type calcium channels are clustered on developing central axons

We examined the expression of various calcium channel α_1 subunits in developing white matter and detected a clustered expression pattern of α_{1A} (P/Q-type: Figs 4A and B, and 5A) and α_{1C} (L-type: Figs 4A and 5B) subunits (α_{1B} and α_{1D} were not detected, data not shown). While α_{1C} clusters were present at a relatively stable level between P2–P20, α_{1A} clusters were almost absent at P2, reached a maximum at P12 and declined by P20 (Figs 4A, and 5A and B). Calcium channel clusters were co-localized with small NF-70(+) axons (Fig. 4B), and were less numerous on larger NF-200(+) axons (data not shown). Small diameter developing axons are close-packed and as a result single NF-70(+) axons are difficult to resolve at the light level. To test whether overlap of the α_{1A} clusters with the NF-70 immuno-staining was significant rather than a random event, we blind-counted the extent of α_{1A} –NF-70 overlap in normal images and in images with the α_{1A} rotated by 90 deg, revealing $63.4 \pm 5.1\%$ ($n = 8$) co-localization in rotated compared to $87.1 \pm 2.6\%$ ($n = 9$, $P < 0.001$) in the non-rotated images (Fig. 4D). Similar levels of co-localization were detected for α_{1C} –NF-70 ($P < 0.001$, Fig. 4E). Little co-localization was apparent between either α_{1A} or α_{1C} and the glial markers CNPase (Fig. 4C) or GFAP (Supplemental Fig. 1e–g), and no significant difference was found in the degree of overlap between normal and rotated images ($P > 0.05$ in all cases, Supplemental Fig. 1h and i). In control experiments, α_{1A} clusters were abolished by pre-incubating the antibody with a blocking peptide, or by omitting the primary antibody during co-labelling experiments (Supplemental Fig. 1b–d). Confirmation of the clustered α_{1A} staining of axons was obtained using a second α_{1A} antibody from a different source (Sigma UK; data not shown).

The antibody staining indicated that Ca^{2+} channels appear in clusters on central axons before Na^+ channel clusters first appear (Figs 4A, and 5A and B). We therefore co-stained for α_{1A} and α_{1C} subunits and CASPR-1,

Figure 5. Voltage-gated Ca^{2+} channel clusters on developing central axons are precursors of nodes of Ranvier

A, α_{1A} subunits (green) are present in clusters in P2 optic nerve, increase in number at P12 but are largely absent at P20 (although diffuse staining remains). Na^+ channels (Nav) clusters (red) are present at P12 and P20. B, α_{1C} subunits (green) are present at a low density throughout the postnatal ages studied. Nav (red) clusters are visible at P12 and P20. C, α_{1A} clusters (green) are associated with CASPR-1 clusters (red) at P9 (two left panels) and P12 (right panel). D, α_{1C} clusters (green) are associated with CASPR-1 immunoreactivity (red) at P9 (two left panels) and P12 (right panel). E, rotating the CASPR-1 images by 90 deg relative to the α_{1A} images (left) or α_{1C} (right) significantly reduced the association between α_1 and CASPR-1 clusters ($***P < 0.001$, normal *versus* rotated), indicating a greater association than would be due to chance. All scale bars, $10 \mu\text{m}$.

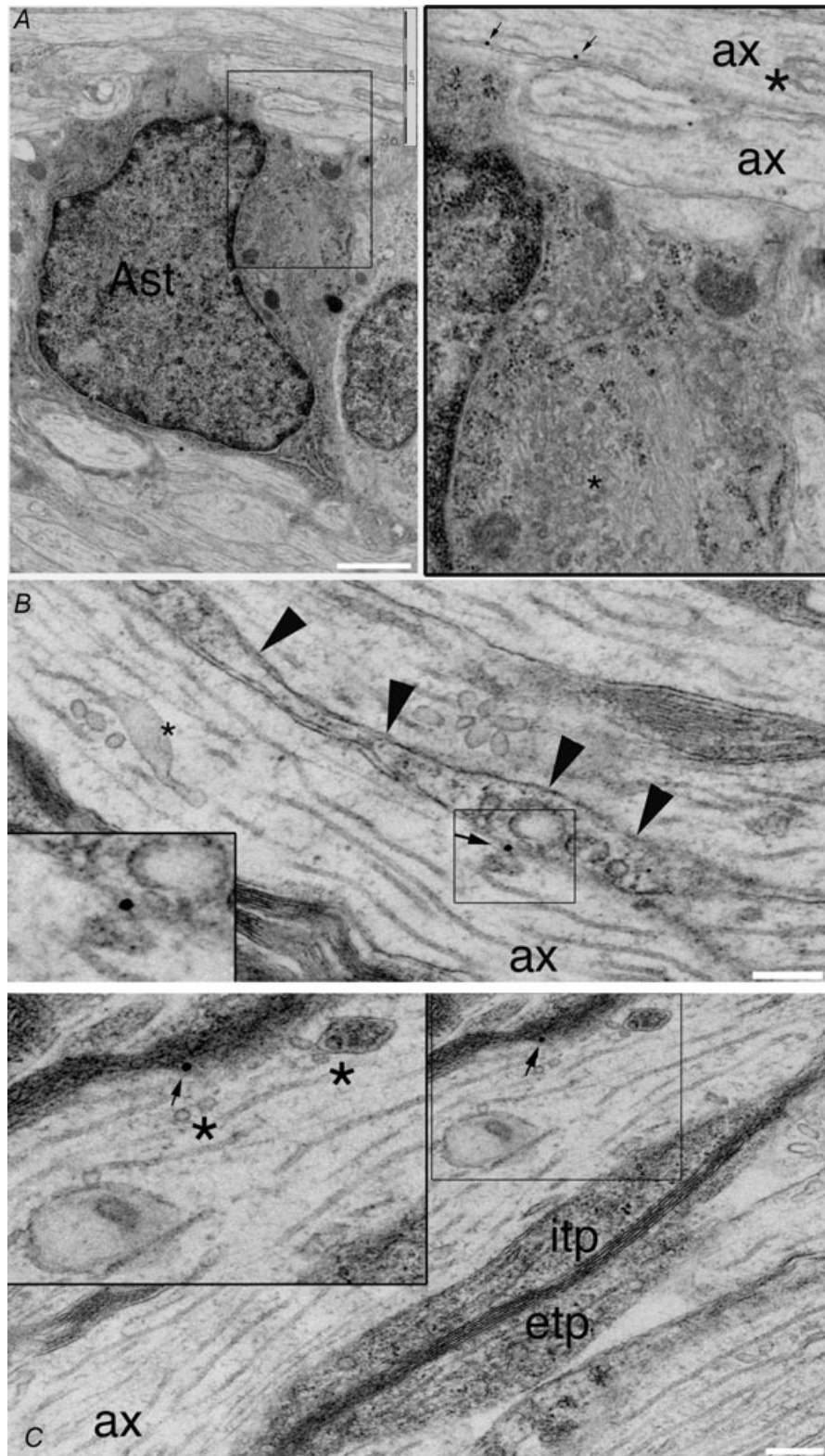


Figure 6. α_{1A} subunits are present on the axolemma of developing axons

A, immuno-gold labelling of α_{1A} protein reveals gold particles on the intracellular face of the axolemma of axons in P10 rat optic nerve (arrows, shown at higher gain to the right). α_{1A} immunoreactivity is present on an unmyelinated axon that is being contacted by an astrocyte (Ast: identified using standard ultrastructural criteria). Note the large vesiculotubular complex vacuole (asterisk) in the axon (ax). *B*, an unmyelinated axon (ax) with a glial process running parallel to the axolemma (arrow heads) has immuno-gold labelling of α_{1A} protein at a point

an early component of the node of Ranvier (Rasband & Shrager, 2000). α_{1A} clusters were co-localized with $12.2 \pm 0.5\%$ of CASPR-1 clusters and were adjacent with a further $43.5 \pm 0.8\%$ (16 fields of view, 5 nerves) at P9 (Fig. 5C and E). By P12, $22.2 \pm 1.6\%$ of α_{1A} clusters were co-localized with CASPR-1 clusters and $35.2 \pm 1.7\%$ were adjacent (12 fields of view, 4 nerves) (Fig. 5C and E). A similar pattern of expression was seen for clusters of α_{1C} subunits (Fig. 5D and E). In all cases, the degree of association was significantly greater than that found in rotated controls ($P < 0.001$, Fig. 5E). In contrast to CASPR-1, only $22.5 \pm 3.3\%$ of Na^+ channel clusters were associated (overlap + adjacent) with α_{1A} clusters at P12 (4 fields of view, 4 nerves) with very little actual overlap (2.8%). α_{1A} clusters therefore appear several days before Na^+ channel clusters are evident at sites on central axons where nodes are forming, and disperse once Na^+ channel clusters appear.

α_{1A} subunits are localized to the axolemma

At the ultrastructural level, white matter α_{1A} protein was largely restricted to the axolemma and axoplasm of developing axons. Immuno-gold particles were particularly common at zones where glial processes were making contact with axons (Fig. 6), areas that were also rich in sites where the vesiculotubular complex appeared to be fusing or approaching the axolemma. Blinded counting of all the gold particles within eight randomly selected whole grid sections revealed that 69.0% of the axolemma particles were located at sites where vesicular fusion was occurring, defined as regions where axoplasmic vesicles or tubules were closely associated with the axolemma ($n = 54$ gold particles in total). The mean distance to the nearest fusion zone for the remaining 31.0% of particles was $0.42 \mu\text{m}$. Analysis revealed that $30.9 \pm 2.8\%$ of axolemma area was associated with vesicle fusion sites at P8–P12 (47 axons examined in the same 8 grid sections), and the high coincidence of α_{1A} particles and vesiculotubular complex fusion sites is not due to chance alone ($P < 0.001$). Of the particles that were located at or near fusion sites, 93.0% were found at points where glial cell processes were directly apposed to the axolemma. In 37.0% of these cases the glial process was myelinating the axon, and the remaining 63.0% of the peri-axonal glial processes were either non-myelinating oligodendrocyte or astrocyte processes, which are often hard to differentiate.

Vesiculotubular complex is a poorly defined but significant component of developing central axons (Hildebrand & Waxman, 1984), and probably contains elements of tubulovesicular organelles transported from the somata (Nakata *et al.* 1998), in addition to 'axoplasmic reticulum' (Lindsey & Ellisman, 1985), but it is probably not limited to these. The vesiculotubular complex is thought to be involved in trafficking of components to the axolemma during axonal diameter expansion, and is less apparent in mature axons (Hildebrand & Waxman, 1984). An analysis of axons in the P8–P12 optic nerve revealed that prior to the initiation of glial contact $20.3 \pm 4.0\%$ ($n = 13$ axons) of the axolemma was associated with apparent vesiculotubular complex fusion sites. This proportion significantly increased to $31.5 \pm 4.2\%$ in more mature axons that had glial processes aligned along the axolemma ($n = 15$, $P < 0.001$), and to $38.0 \pm 4.5\%$ in axons with layers of compact myelin ($n = 19$, $P < 0.001$). By P20 the proportion of the axolemma exhibiting fusion sites in myelinated axons fell to $23.1 \pm 3.1\%$, which was significantly lower than that in myelinating P8–P12 axons ($n = 32$, $P < 0.001$), confirming the relationship between the onset of myelination, axon diameter expansion and fusion of the vesiculotubular complex to the axolemma. Tubular elements of this structure can range in diameter between 20 and 40 nm and measure up to $25 \mu\text{m}$ in length, making them difficult to distinguish from microtubules. Vesicular elements can range between tens to several hundreds of nanometres across (e.g. Fig. 6 and Supplemental Fig. 2), and in the current study we found that both vesicular and tubular elements appear to fuse to the axolemma in places (Fig. 6).

Since the α_{1A} protein is located at regions where vesiculotubular complex elements are fusing with the axolemma, we probed for other components of synaptic vesicle targeting in developing central axons. Using immuno-electron microscopy, we found SNAP-25 expression in a similar pattern to α_{1A} (Fig. 7A and B), with 71.2% of gold particles located on the interior axolemma surface (25% on vesiculotubular complex, 3.8% in the cytoplasm; 49 micrograph fields analysed). In contrast, expression of the vesicular ATPase (V-ATPase) was a mirror image of this pattern (Fig. 7C–E) with 75.8% present in the vesiculotubular complex (12% on the interior axolemma, 10.5% in the cytoplasm; 54 micrograph fields). V-ATPase is involved in glutamate loading of synaptic vesicles and glutamate was found to be concentrated in the vesiculotubular complex (Fig. 7F and

where an element of the vesiculotubular complex appears to be fusing with the axolemma (shown at higher gain in the box). A prominent component of the vesiculotubular complex present in the centre of the axon is indicated by an asterisk. C, vesicle elements of the vesiculotubular complex (asterisk) appear to be approaching and fusing with the axolemma at a point where α_{1A} protein is detected by immuno-gold labelling (arrow). This axon is being myelinated and has prominent oligodendrocyte interior and exterior tongue processes (itp, etp). Scale bars: A, 500 nm; B and C, 200 nm.

G), including within vesiculotubular complex elements fusing with the axolemma (Fig. 7G). Vesiculotubular complex was highlighted in micrographs by intensity thresholding, revealing that 33.1% of the axoplasmic area was taken up by vesiculotubular complex measured in this way (which does not effectively exclude all the microtubules; 49 micrograph fields). Of the gold particles in

glutamate immuno-labelled sections 94.4% were in direct contact with vesiculotubular complex highlighted in this fashion, consistent with significant glutamate enrichment in the vesiculotubular complex. Glutamate reactivity was also detected in glial somata and in their primary processes close to the somata (not shown), but glutamate staining was infrequent in glial processes neighbouring

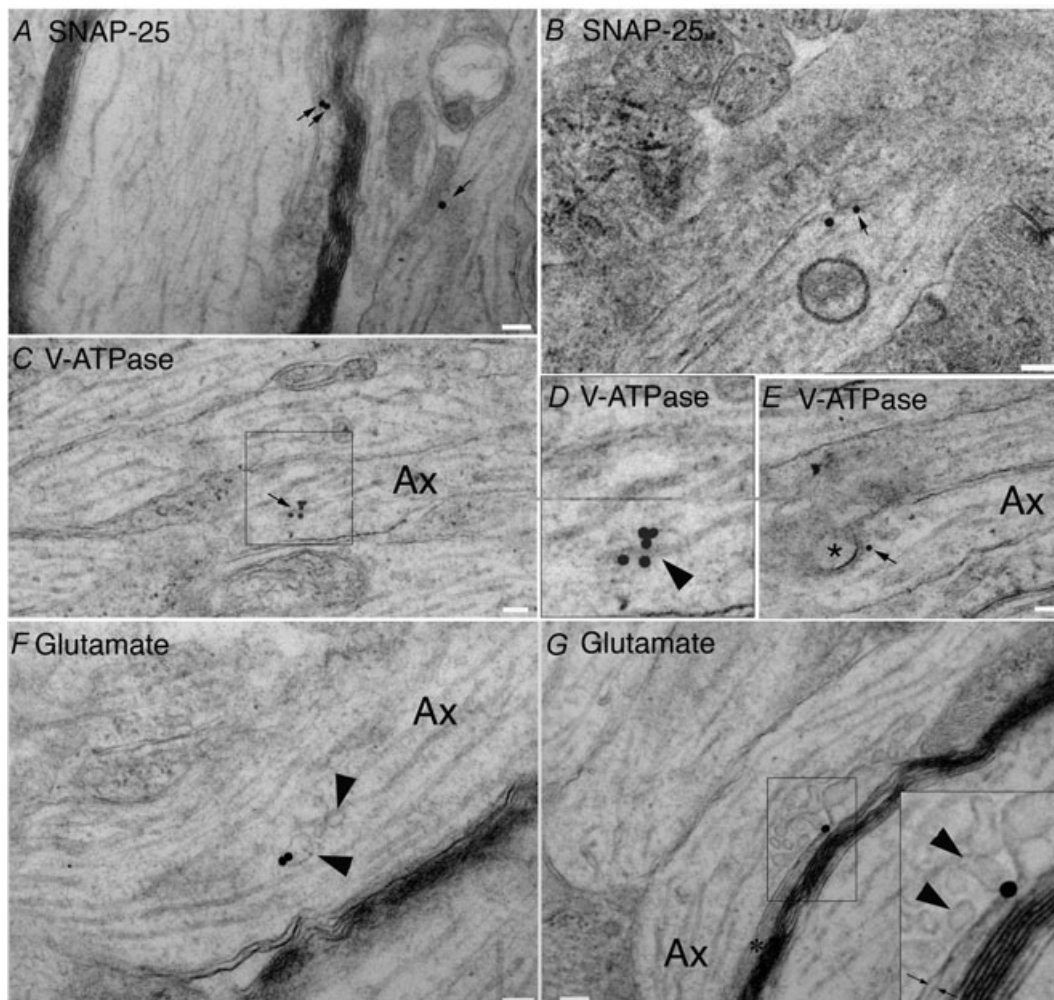


Figure 7. Elements involved in vesicular docking are present in developing axons

A and *B*, SNAP-25 localization in P10 rat optic nerve axons detected with immuno-gold labelling. Gold particles (arrows) are concentrated on the interior face of the axolemma, in particular at regions where elements of the vesiculotubular complex are close to, or appear to have docked with, the axolemma. Note in *A* that gold staining is apparent both in a region where a tubular element is contacting the axolemma (left arrows) and in a region where vesicles appear to be fusing with the axolemma (right arrow). Note in *B* that a large axoplasmic vesicle is apposed to a region with two gold particles on the axolemma (compare this micrograph with *E* below). *C–E*, V-ATPase is densely expressed in elements of the vesiculotubular complex. Note in *C* the intense gold labelling of a tubular element, shown in greater magnification in *D* (box) indicated by an arrow head and having a diameter and morphology that distinguishes it from a microtubule. Note in *E* that staining is apparent on what appears to be a large vesicle in the process of fusing with the axolemma. *F*, glutamate reactivity in a vesicular element of the vesiculotubular complex (arrowheads). *G*, glutamate reactivity in vesicular elements of the vesiculotubular complex (arrow heads) that are in the process of fusing with the axolemma, as shown at higher magnification in the box where vesicular and axolemma membranes can be seen to be contiguous. The vesicles are fusing in an area tightly apposed to a glial process (asterisk) and the immuno-gold particle is located in the extracellular space where the vesicles contents are likely to be released (arrows). Scale bar, 100 nm throughout.

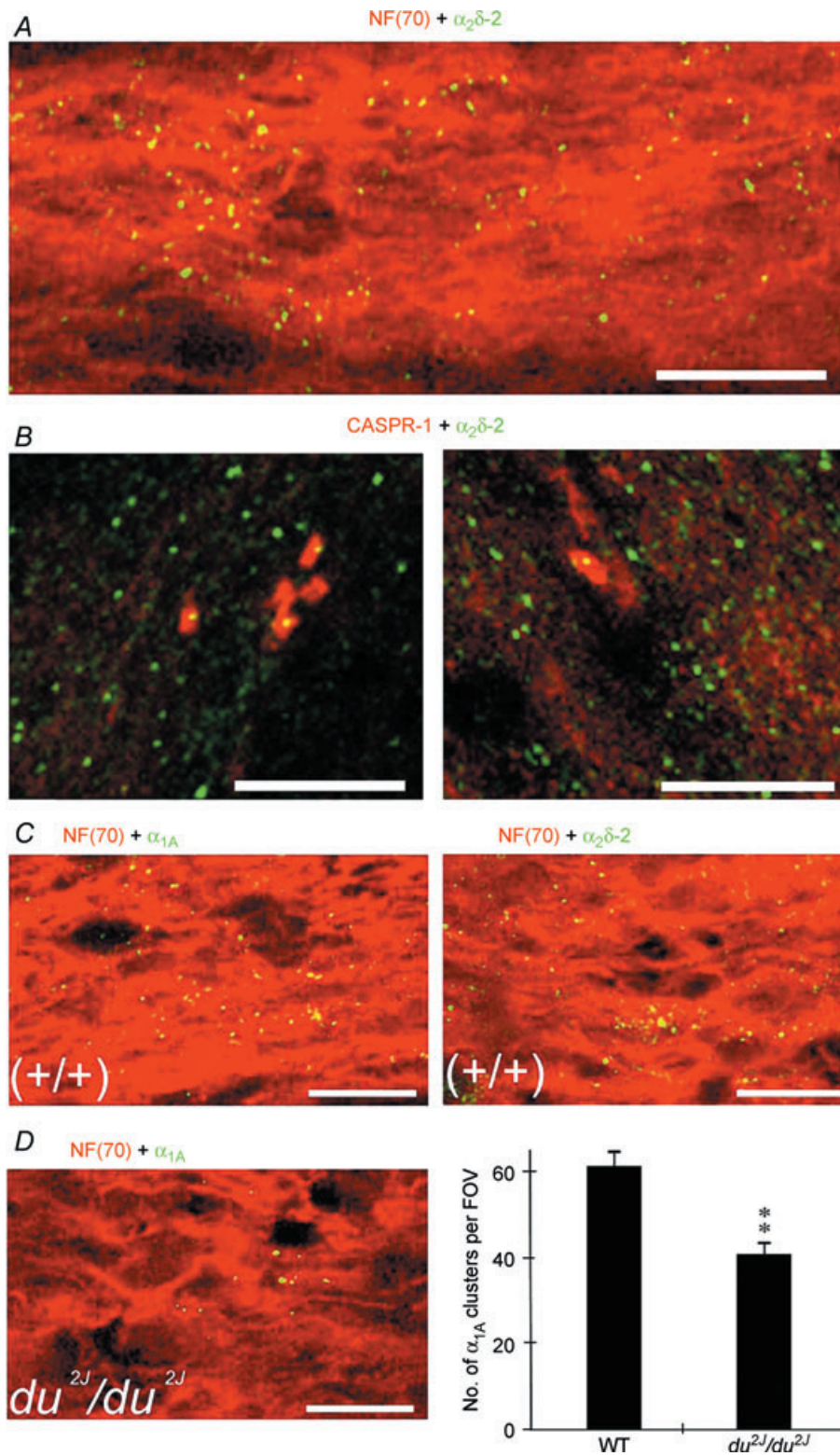
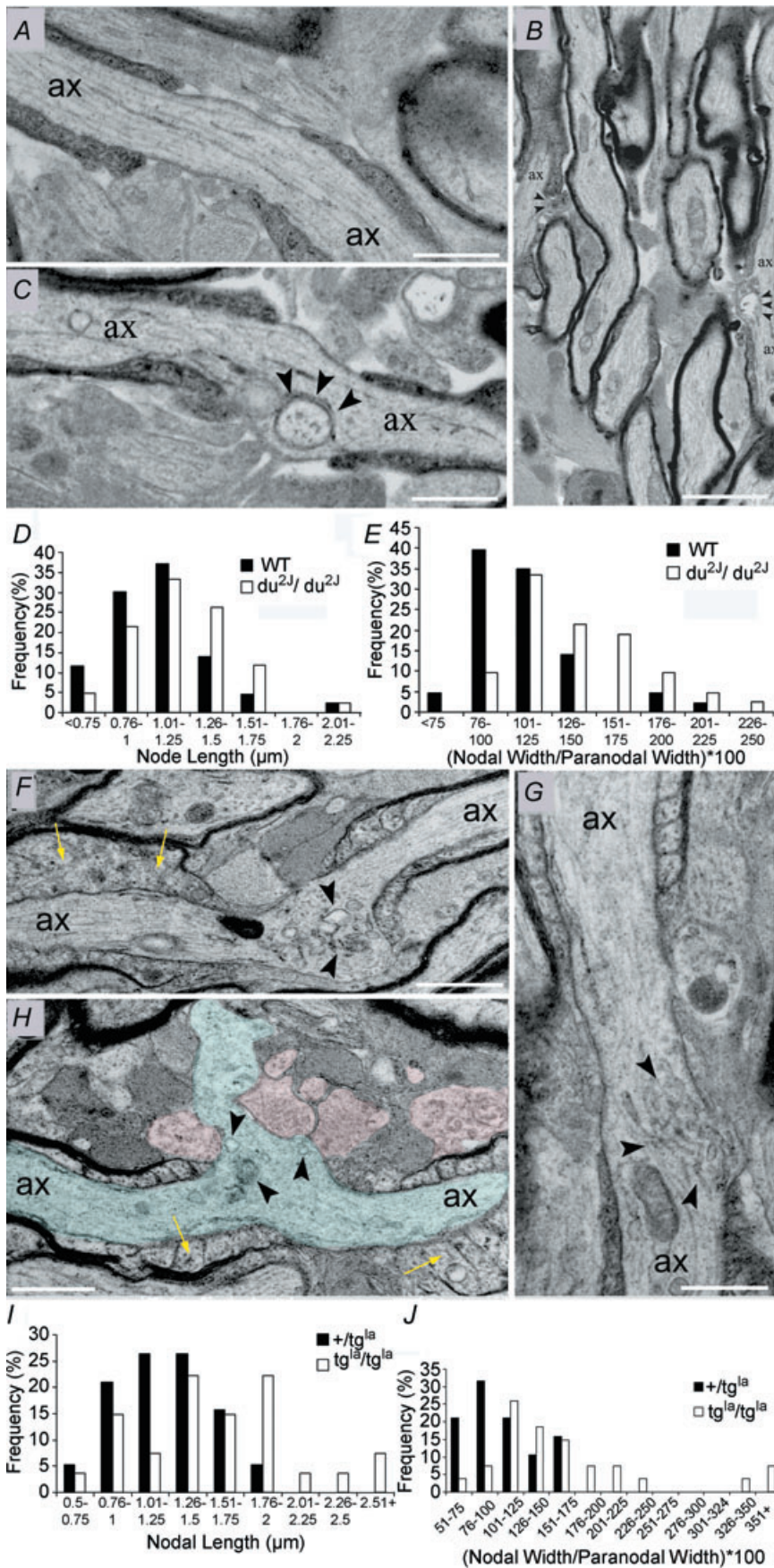


Figure 8. $\alpha_2\delta-2$ subunits are present in clusters on developing central axons

A, $\alpha_2\delta-2$ (green) and NF-70 (red) expression in P12 rat optic nerve. Note that $\alpha_2\delta-2$ clusters are present along NF-70 axons. B, $\alpha_2\delta-2$ clusters (green) are associated with CASPR-1 clusters (red) in P9 (left) and P12 (right) rat optic nerve. C, α_{1A} (green, left) and $\alpha_2\delta-2$ (green, right) co-localize with NF-70(+) axons (red) in P9^{+/+} mouse optic nerve. D, fewer α_{1A} clusters (left, green) are apparent in axons (red) in the du^{2J} mouse, which was statistically significant (right). ***P* < 0.01. Scale bars, 10 μ m.



developing axons, and glutamate was not seen in vesicular structures in any other cellular compartment within white matter other than the vesiculotubular complex. SNAP-25, V-ATPase and glutamate gold-labelling of this type was seen in small diameter yet-to-be-myelinated axons through to large diameter axons with multiple myelin wraps (e.g. SNAP-25 staining in Fig. 7A and B).

Calcium channel mutants have disrupted nodes of Ranvier

As P/Q-type channels were the most abundant channel subtype in developing optic nerve axons and were maximally expressed at a crucial point in maturation we sought evidence of their potential role from two mice strains carrying mutations affecting P/Q-type voltage-gated calcium channels. Ducky (*du*) and ducky-2J (*du^{2J}*) mice carry functionally null mutations in the *Cacna2d2* gene encoding the $\alpha_2\delta$ -2 calcium channel subunit, resulting in reduced P/Q currents in cells expressing these subunits (Barclay *et al.* 2001; Brodbeck *et al.* 2002). Expression of $\alpha_2\delta$ -2 was examined in P12 rat optic nerve and showed a similar clustered expression on NF-70(+) axons to that seen for the α_{1A} and α_{1C} subunits (Fig. 8A). The $\alpha_2\delta$ -2 clusters also had a similar association with CASPR-1 to that seen for α_{1A} clusters at P9 and P12 in the rat (Fig. 8B). At P9 $41.9 \pm 0.4\%$ ($n = 10$) of CASPR-1 clusters were associated with $\alpha_2\delta$ -2 clusters and $51.2 \pm 2.6\%$ ($n = 9$) of CASPR-1 clusters were associated with $\alpha_2\delta$ -2 clusters at P12. Similar clustered expression of α_{1A} and $\alpha_2\delta$ -2 was also common in NF-70(+)^{+/+} mouse optic nerve axons (Fig. 8C), while the number of α_{1A} clusters was significantly reduced in *du^{2J}/du^{2J}* optic nerve compared to their *+/+* littermates ($P < 0.01$, Fig. 8D). As the $\alpha_2\delta$ -2 subunit is thought mainly to enhance α_{1A} expression with only minor effects on gating, this down-regulation of α_{1A} clusters in *du^{2J}/du^{2J}* is in line with the $\sim 30\%$ loss of P/Q conductance in Purkinje cells of both *du/dμ* (Barclay *et al.* 2001; Brodbeck *et al.* 2002) and in *du^{2J}/du^{2J}* (Donato *et al.* 2006).

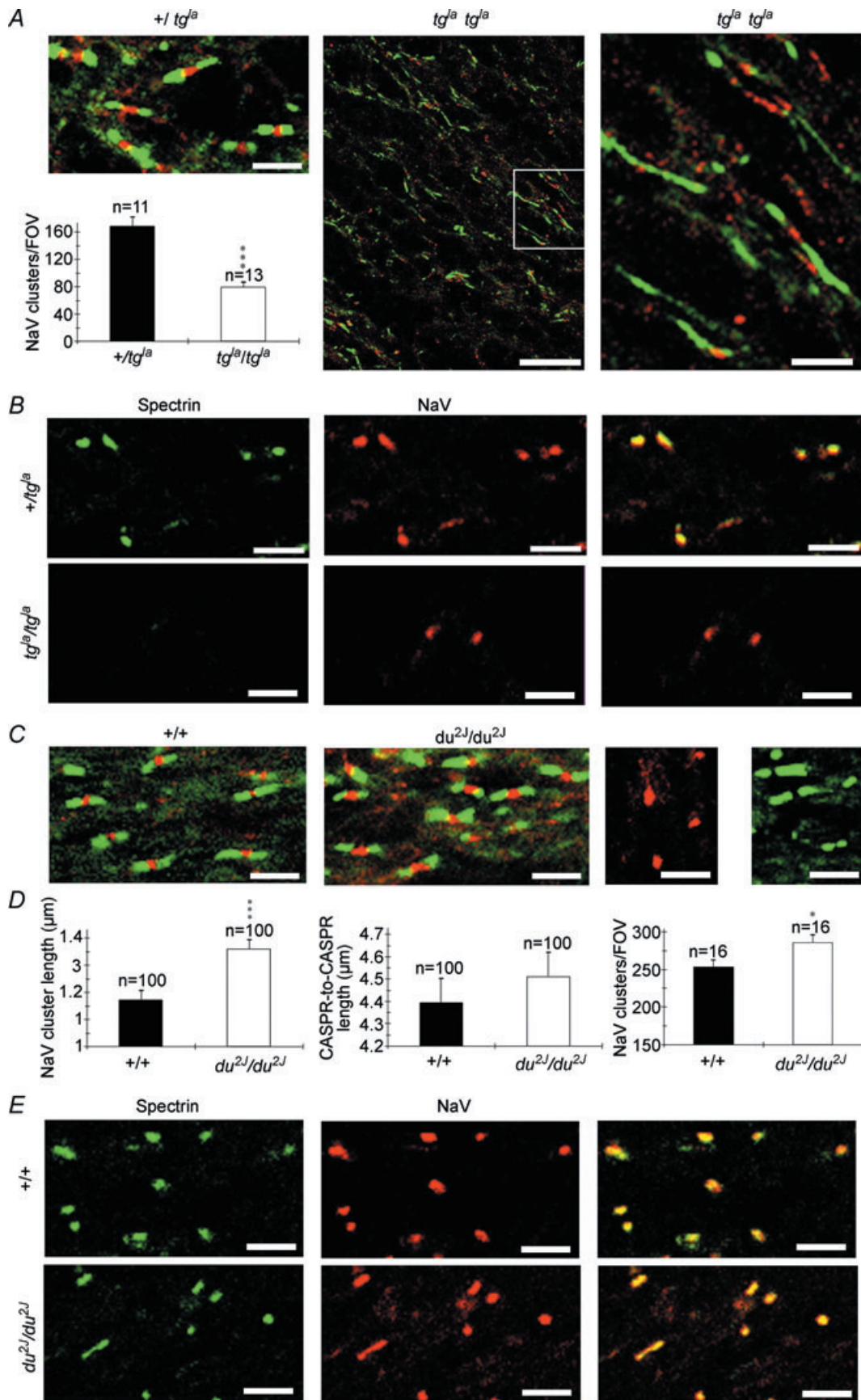
Since α_{1A} clusters were reduced in *du^{2J}/du^{2J}* we examined the morphology of the optic nerve nodes of

Ranvier in these animals at $\sim P25$. No obvious differences were found in cross-sections of control *+/+* littermates and *du^{2J}/du^{2J}* (not shown), and the *+/+* animals displayed normal nodal morphology for this point in development when examined in long section, with end-loops of the myelinating sheath framing a clear nodal gap (Fig. 9A, $n = 43$ nodes examined). In contrast, the nodes of Ranvier of *du^{2J}/du^{2J}* animals ($n = 42$ nodes examined) had a significantly extended nodal length (Fig. 9D; $1.07 \pm 0.05 \mu\text{m}$ in wild-type *versus* $1.2 \pm 0.05 \mu\text{m}$ in *du^{2J}/du^{2J}*, $P < 0.05$), and a significantly expanded nodal width, as determined by measuring the diameter of the node *versus* the diameter of the paranode to account for differences in axon size (Fig. 9E; $111 \pm 4\%$ in wild-type *versus* $139 \pm 5\%$ in *du^{2J}/du^{2J}*, $P < 0.001$). No significant difference in axon or fibre diameter were found between *+/+* and *du^{2J}/du^{2J}*; however, a significant decrease in the g value (axon diameter/fibre diameter) was found (0.79 ± 0.005 , $n = 70$, in wild-type *versus* 0.76 ± 0.006 in *du^{2J}/du^{2J}*, $n = 119$, $P < 0.01$). The aberrant nodes of the *du^{2J}/du^{2J}* animals typically contained large vesicular inclusions under the nodal membrane (Fig. 9B and C), while the remaining nodes exhibited a range of malformations from swelling of the nodal membrane to the presence of vacuoles and other inclusions within the nodal axoplasm.

We also examined node morphology in the *leaner* (*tg^{la}/tg^{la}*) mutant, which has a mutation in the *Cacna1a* gene encoding the α_{1A} subunit. *tg^{la}/tg^{la}* has more severely compromised P/Q channel function than *du^{2J}/du^{2J}*, corresponding to a 60–70% reduction in peak P-type current density in Purkinje cells (Lorenzon *et al.* 1998; Fletcher *et al.* 1996; Dove *et al.* 1998; Wakamori *et al.* 1998). While optic nerves from control (*+/tg^{la}*) littermates (used as control since *leaner* is bred on oligosyndactylism (*Os*) background, and *Os/Os* is fatal) appeared normal, *tg^{la}/tg^{la}* optic nerves had regions of mild and severe malformation throughout. Regions of severe injury were infiltrated with activated microglia (Supplemental Fig. 3), indicating an ongoing pathology. We examined regions of mild injury to look for the initial changes in axons before wide-scale pathology was evident. Nodes of Ranvier in *tg^{la}/tg^{la}*

Figure 9. Ultrastructural correlates of P/Q channel dysfunction in developing central axons

A–E, *du^{2J}/du^{2J}*; F–J, *tg^{la}/tg^{la}*. A, long-section of a P25^{+/+} optic nerve axon (ax) showing a typical node of Ranvier. Note the normal nodal membrane that separates the myelin end-loops and the typical appearance of the nodal and paranodal glial processes. B, two nodes are present in this lower power micrograph of P25 *du^{2J}/du^{2J}* optic nerve. In both cases, vacuoles of various sizes are present in the nodal axoplasm (arrow heads). C, long section of a node from P25 *du^{2J}/du^{2J}* optic nerve. Note the presence of large vacuoles within the nodal axoplasm adjacent to the axolemma (indicated by arrowheads). D, comparison of the node length in *+/+* (WT) and *du^{2J}/du^{2J}* optic nerve. E, comparison of the node diameter ((node width/paranodal width) \times 100) in *+/+* and *du^{2J}/du^{2J}*. F and G, long sections of nodes of Ranvier in *tg^{la}/tg^{la}*. Note the presence of vacuoles of various sizes and shapes within the nodal axoplasm (arrowheads). The nodal axolemma was generally wider in the mutant and in some cases had become extruded into the extra-nodal space (H, axon shaded blue). Paranodal glial processes were often abnormal (e.g. H: shaded red), and paranodal end loops appeared swollen in places (yellow arrows). I, comparison of the node length in *+/tg^{la}* and *tg^{la}/tg^{la}* optic nerve. J, comparison of the node diameter in *+/tg^{la}* and *tg^{la}/tg^{la}*. Scale bars: A, C, F and G, 2 μm ; B, 5 μm .



axons were often malformed and contained numerous vesicular inclusions (Fig. 9F–H). Malformations ranged from a marked distension of the nodal membrane (Fig. 9F), to complete herniation of inclusion-loaded axoplasm through the paranodal glial processes (Fig. 9H, shaded blue). Swollen and electron lucent peri-nodal glial processes were often seen in these malformed nodes (Fig. 9H, shaded red), and while there was not detachment or disintegration of the myelin end-loops, they often appeared swollen. Compared to controls, nodes of tg^{la}/tg^{la} animals were significantly longer (Fig. 9I; 1.25 ± 0.07 , $n = 19$, versus $1.6 \pm 0.1 \mu\text{m}$, $n = 26$, $P < 0.05$) and wider (Fig. 9J; 1.06 ± 0.07 , $n = 19$ in $+/tg^{la}$ versus 1.77 ± 0.02 , $n = 27$, $P < 0.01$). Morphometric analysis of myelinated axons also revealed significant decreases in axon diameter ($0.96 \pm 0.03 \mu\text{m}$ $+/tg^{la}$, $n = 70$, versus $0.82 \pm 0.03 \mu\text{m}$ in tg^{la}/tg^{la} , $n = 105$, $P < 0.05$) and fibre diameter ($1.18 \pm 0.03 \mu\text{m}$ $+/tg^{la}$, $n = 70$, versus $1.01 \pm 0.03 \mu\text{m}$ in tg^{la}/tg^{la} , $n = 105$, $P < 0.01$) in tg^{la}/tg^{la} animals. The calculated g value was not significantly affected by the mutation (0.81 ± 0.005 , $n = 70$, versus 0.79 ± 0.006 , $n = 105$, $P > 0.05$).

The distribution of nodal proteins was examined in du^{2j}/du^{2j} and tg^{la}/tg^{la} , revealing a significant reduction in sodium channel clusters and a marked displacement of CASPR-1 along axons in tg^{la}/tg^{la} animals compared to control (Fig. 10A). Regions of elongated CASPR-1 expression were sometimes punctuated by sodium channel clusters, but not on all occasions. While β IV spectrin and sodium channel clustering appeared normal on the $+/tg^{la}$ controls, there was no detectable β IV spectrin co-localized with the remaining sodium channel clusters in tg^{la}/tg^{la} (Fig. 10B). Less marked changes were apparent in du^{2j}/du^{2j} and included a significant increase in the sodium channel cluster length (Fig. 10C–E).

Discussion

The results presented here show that developing central axons express functional voltage-gated calcium channels

that, since they contribute to action potential propagation, must mediate a significant inward calcium current during the action potential. The L-type and P/Q-type channels involved are expressed in a clustered pattern along immature axons, and the α_{1A} subunits that form P/Q channels are transiently clustered in the axolemma at sites where the underlying vesiculotubular complex is fusing with the axolemma, which includes regions where node of Ranvier formation is underway. Vesiculotubular complex is a poorly defined axoplasmic component of developing central axons and includes both tubular and vesicular elements (Hildebrand & Waxman, 1984; Lindsey & Ellisman, 1985; Nakata *et al.* 1998). In the current study, both tubular and vesicular elements appeared to fuse with the axolemma in regions rich in α_{1A} expression, regions that also had a high coincidence with the presence of glial processes aligned to the extracellular surface of the axolemma. While the vesiculotubular elements are larger and lack the classic features of synaptic vesicles, they did express some of the molecular components of synaptic vesicle fusion such as V-ATPase and the excitatory neurotransmitter glutamate, while the axolemma was shown to contain a high density of SNAP-25, a component of the vesicular docking machinery. Mutations of the α_{1A} subunit, or the $\alpha_2\delta$ -2 subunit also shown to be present at early node sites, resulted in the malformation of nodes of Ranvier featuring loss of nodal protein localization, disruption of the nodal membrane and a build-up of vesicles under the nodal axolemma. The presence of the various components of vesicular fusion throughout the development of myelination is consistent with a role for vesicular glutamate release in the co-ordination of myelination and node of Ranvier formation.

The effects of P/Q channel mutation upon node of Ranvier development is either a direct effect associated with a disruption in vesicle docking at the nodal axolemma, or an indirect effect possibly following a reduction in axonal excitability. Thus, a reduction in current through P/Q channels might produce a decline in the rate of action potential discharge down optic

Figure 10. P/Q channel dysfunction is associated with a disruption in the localization of nodal proteins
 A and B, tg^{la}/tg^{la} ; C–E, du^{2j}/du^{2j} . A, top, left: NaV (red) and CASPR-1 (green) localization in control ($+/tg^{la}$) optic nerve. Bottom, left: the density of NaV clusters is significantly lower in tg^{la}/tg^{la} optic nerve than in $+/tg^{la}$. Middle: NaV (red) and CASPR-1 (green) localization in tg^{la}/tg^{la} optic nerve. Note the grossly elongated regions of CASPR-1 localization and the sparse, ectopic nature of the NaV clusters (the box is shown in higher magnification to the right). B, β IV-spectrin (green) and NaV (red) clusters are co-localized in control ($+/tg^{la}$) optic nerve (top) but no β IV-spectrin reactivity is found in tg^{la}/tg^{la} optic nerve (bottom). Overlaid images are shown to the right. C, left, NaV (red) and CASPR-1 (green) localization in control ($+/+$) optic nerve. Middle: NaV (red) and CASPR-1 localization in du^{2j}/du^{2j} optic nerve. Note the similarity in the staining patterns. Right: two control images showing the absence of CASPR-1 reactivity when the CASPR-1 antibody is omitted from the staining protocol (red, NaV staining remains), and the absence of NaV reactivity when the NaV antibody is omitted from the staining protocol (green, CASPR-1 staining remains). D, the length of NaV clusters (left), the distance between CASPR-1 clusters at nodes (middle, measured from the juxta-paranodal end of one CASPR-1 cluster to the juxta-paranodal end of its companion cluster), and the density of NaV clusters (right) in $+/+$ and du^{2j}/du^{2j} optic nerve. E, spectrin (green) and NaV (red) staining is co-localized in both $+/+$ (top) and du^{2j}/du^{2j} (bottom) optic nerve. Overlaid images are shown to the right. * $P < 0.05$, *** $P < 0.001$. Scale bars, all $5 \mu\text{m}$, apart from middle panel in A, $20 \mu\text{m}$.

nerve axons, either due to a loss of inward calcium current during action potential propagation, or following a reduction in synaptic input to the retinal ganglion cell somata. While a loss of axon excitability such as this might affect axon development, it seems unlikely to underlie the disruption of node of Ranvier formation seen in the current study. It has been shown, for example, that complete block of electrical activity in the optic pathway has no comparable effect upon the development of the node, although it does have profound effects upon peri-axonal glial cell processes (Friedman & Shatz, 1990), that were not seen in the current study. It is more likely, therefore, that the effects of P/Q channel mutation upon node development arise from disruption of tubular-vesicular docking and the subsequent interruption in the supply of membrane proteins necessary for node of Ranvier development, and/or from the failure of a signalling pathway mediated by vesicular release from the nodal axolemma. The presence of V-ATPase and glutamate in the vesiculotubular complex, and of SNAP-25 in the axolemma, indicate that vesicular fusion triggered by calcium influx through calcium channels will liberate glutamate onto the closely associated oligodendrocyte processes. Recently, Kukley *et al.* (2007) and Ziskin *et al.* (2007) have reported vesicular release of glutamate from both developing and mature central axons, leading to the activation of AMPA/kainate receptors on neighbouring NG2(+) cells. Ziskin *et al.* (2007) suggest that these AMPA/kainate receptor-mediated currents may have a role in stimulating differentiation of the cells into oligodendrocytes, while Kukley *et al.* (2007) speculate that glutamate release may provide a signal capable of directing oligodendrocytes to axons. Indeed, it is known that oligodendrocyte migration, differentiation and survival are regulated by non-NMDA-type glutamate receptors (Gallo & Ghiani, 2000), and recent findings have highlighted the presence of NMDA-type glutamate receptors on early oligodendrocyte processes and within myelin itself (Káradóttir *et al.* 2005; Salter & Fern, 2005; Micu *et al.* 2006). Such receptors are ideally located to receive vesicular glutamate released from developing axons, and indeed glutamatergic postsynaptic potentials are observed in white matter oligodendrocytes (Káradóttir *et al.* 2005). White matter contains no synaptic boutons, and taken together, the data strongly suggest that axons are the synaptic partners of oligodendrocytes, at least during myelination.

Signalling pathways between axons and oligodendrocytes are known to be important in myelination (Demerens *et al.* 1996; Stevens *et al.* 1998). The glutamatergic signalling pathways described by Ziskin *et al.* (2007) and Kukley *et al.* (2007) are consistent with the current findings of glutamate-rich vesicular elements within developing axons, synaptic proteins on these structures and on the axolemma, and the requirement

of functional axonal synaptic-type calcium channels for proper node of Ranvier formation. A pathway of this type may act in parallel to the recently reported leukaemia inhibitory factor-mediated (LIF) signalling pathway involving axons and astrocytes (Ishibashi *et al.* 2006). Interruption of a glutamatergic pathway in *leaner* can be expected to influence the relationship between axons and their myelinating oligodendrocyte processes. Indeed, dysmyelinated oligodendrocyte phenotypes such as the *shiverer* (lacking myelin basic protein) and *myelin-deficient* (*md*) mutants exhibit a similar disruption in CASPR-1 expression to that found in *leaner* in the current study, and have a similar reduction in sodium channel clusters (Kaplan *et al.* 1997; Rasband *et al.* 1999; Tait *et al.* 2000; Boiko *et al.* 2001; Arroyo *et al.* 2002). A direct effect of calcium channel dysfunction upon protein targeting to the node can not be discounted, since axons lacking scaffold elements such as ankyrin G and β IV spectrin have reduced sodium channel clusters and the presence of vacuoles in the nodal axoplasm (e.g. Komada & Soriano, 2002; Yang *et al.* 2004).

Several other spontaneous mutations with compromised P/Q channel function have been identified in addition to *du^{2l}/du^{2l}* and *tg^{la}/tg^{la}*. Of these, *duky* (*du/d μ*), *tottering* (*tg/tg*) and *tottering/leaner* (*tg/tg^{la}*) show marked malformation of axon tracts (Meier, 1968; Meier & MacPike, 1971; Rhyu *et al.* 1999a). While abnormal axons have also been described in P/Q null mice (Jun *et al.* 1999) and the *rolling* (*tg^{rol}/tg^{rol}*) mutation (Rhyu *et al.* 1999b), gross disruption of white matter has not been reported in these or other P/Q mutants. The phenotype of P/Q mutants is highly variable (Fletcher & Frankel, 1999), which is presumably a product of differences in the effects upon channel function and the degree of compensatory changes in other Ca²⁺ channel types. Of the mutant mice, *tg^{la}/tg^{la}* is reported to have the most compromised function and shows no compensatory increases in other high-voltage-activated Ca²⁺ channels, possibly due to the unaffected level of subunit protein expression in this mutant (Dove *et al.* 1998; Wakamori *et al.* 1998). Large compensatory increases in other high-voltage-activated Ca²⁺ channels have been reported in P/Q null mice (Jun *et al.* 1999; Fletcher *et al.* 2001), which can completely counter the loss of P/Q current in presynaptic nerve terminals (Inchauspe *et al.* 2004). Similar compensatory changes may overcome the loss of axonal P/Q channels in null animals, allowing formation of the node to proceed adequately.

Alongside the important role in nodal development, we have shown that Ca²⁺ channels contribute to action potential conduction at a point when the axon diameter is increasing rapidly (Hildebrand & Waxman, 1984). This is a period when Na⁺ channels are being re-distributed to mediate saltatory conduction (Rasband & Shrager, 2000), but before sufficient compact myelin is present to allow

saltatory conduction to proceed. It has been unclear how axons retain the ability to conduct action potentials as they undergo this transformation but it is essential for proper CNS development that they do so (Shatz, 1996). By boosting inward current during the action potential, Ca^{2+} channels are well placed to counter the temporary biophysical constraints that will inhibit axon function during early myelination. In particular, the P/Q channel expression pattern is ideal to assist with action potential conduction during the period of axon diameter expansion, while the L-type channels may be involved primarily before diameter expansion begins, having a relatively high expression level in P2–P5 axons. Calcium channels may therefore have multiple functions in developing central axons. Two earlier studies failed to report the presence of a significant calcium conductance in developing central axons. Foster *et al.* (1982) did not record a DCAP in the neonatal rat optic nerve following perfusion with isotonic Ba^{2+} . It appears that the rate of stimulation used in this study was 0.5 Hz and our analysis indicates that any DCAP evoked under these conditions would fail after several seconds (see Fig. 2D). Since the recordings collected in this study were averages of eight sweeps, a short-lived DCAP would have been near-impossible to detect. Sun & Chiu (1999) recorded Ca^{2+} influx into regions between neonatal rat optic nerve glia following axonal stimulation. They report effects of L-type calcium channel blockers that did not reach significance given the small number of trials, but may have done with a larger sample size.

Finally, in addition to physiological and developmental roles, axonal calcium channels are likely to be significant for a variety of pathological conditions. The axons of immature white matter are the focus of injury in a number of developmental white matter injuries including periventricular leukomalacia, the main pathology associated with cerebral palsy (Back & Rivkees, 2004). Cerebral palsy is the most common human birth disorder and is thought to be at least partly ischaemic in origin. Since ischaemic axonal injury is largely calcium mediated (Stys *et al.* 1992; Fern *et al.* 1995), calcium channels must represent a major pathway for ischaemic calcium influx into developing central axons.

References

- Aidley DJ (1971). *The Physiology of Excitable Cells*. Cambridge University Press, Cambridge.
- Armstrong CM & Cota G (1999). Calcium block of Na^+ channels and its effect on closing rate. *Proc Natl Acad Sci U S A* **96**, 4154–4157.
- Arroyo EJ, Xu T, Grinspan J, Lambert S, Levinson SR, Brophy PJ, Peles E & Scherer SS (2002). Genetic dysmyelination alters the molecular architecture of the nodal region. *J Neurosci* **22**, 1726–1737.
- Back SA, Craig A, Kayton RJ, Luo NL, Meshul CK, Allcock N & Fern R (2006). Hypoxia-ischemia preferentially triggers glutamate depletion from oligodendroglia and axons in perinatal cerebral white matter. *J Cereb Blood Flow Metab* **27**, 334–347.
- Back SA & Rivkees SA (2004). Emerging concepts in periventricular white matter injury. *Semin Perinatol* **28**, 405–414.
- Barclay J, Balaguero N, Mione M, Ackerman SL, Letts VA, Brodbeck J, Canti C, Meir A, Page KM, Kusumi K, Perez-Reyes E, Lander ES, Frankel WN, Gardiner RM, Dolphin AC & Rees M (2001). Ducky mouse phenotype of epilepsy and ataxia is associated with mutations in the *Cacna2d2* gene and decreased calcium channel current in cerebellar Purkinje cells. *J Neurosci* **21**, 6095–6104.
- Boiko T, Rasband MN, Levinson SR, Caldwell JH, Mandel G, Trimmer JS & Matthews G (2001). Compact myelin dictates the differential targeting of two sodium channel isoforms in the same axon. *Neuron* **30**, 91–104.
- Brismar T & Frankenhaeuser B (1972). The effect of calcium on the potassium permeability in the myelinated nerve fibre of *Xenopus laevis*. *Acta Physiol Scand* **85**, 237–241.
- Brodbeck J, Davies A, Courtney JM, Meir A, Balaguero N, Canti C, Moss FJ, Page KM, Pratt WS, Hunt SP, Barclay J, Rees M & Dolphin AC (2002). The ducky mutation in *Cacna2d2* results in altered Purkinje cell morphology and is associated with the expression of a truncated $\alpha_2\delta_2$ protein with abnormal function. *J Biol Chem* **277**, 7684–7693.
- Brown AM, Westenbroek RE, Catterall WA & Ransom BR (2001). Axonal L-type Ca^{2+} channels and anoxic injury in rat CNS white matter. *J Neurophysiol* **85**, 900–911.
- Callewaert G, Eilers J & Konnerth A (1996). Axonal calcium entry during fast 'sodium' action potentials in rat cerebellar Purkinje neurones. *J Physiol* **495**, 641–647.
- Catterall WA (2000). Structure and regulation of voltage-gated Ca^{2+} channels. *Annu Rev Cell Dev Biol* **16**, 521–555.
- Conklin MW, Lin MS & Spitzer NC (2005). Local calcium transients contribute to disappearance of pFAK, focal complex removal and deadhesion of neuronal growth cones and fibroblasts. *Dev Biol* **287**, 201–212.
- Demerens C, Stankoff B, Logak M, Anglade P, Allinquant B, Couraud F, Zalc B & Lubetzki C (1996). Induction of myelination in the central nervous system by electrical activity. *Proc Natl Acad Sci U S A* **93**, 9887–9892.
- Donato R, Page KM, Koch D, Nieto-Rostro M, Foucault I, Davies A, Wilkinson T, Rees M, Edwards FA & Dolphin AC (2006). The ducky^{2J} mutation in *Cacna2d2* results in reduced spontaneous Purkinje cell activity and altered gene expression. *J Neurosci* **26**, 12576–12586.
- Dove LS, Abbott LC & Griffith WH (1998). Whole-cell and single-channel analysis of P-type calcium currents in cerebellar Purkinje cells of leaner mutant mice. *J Neurosci* **18**, 7687–7699.
- Fabricius M, Fuhr S, Bhatia R, Boutelle M, Hashemi P, Strong AJ & Lauritzen M (2006). Cortical spreading depression and peri-infarct depolarization in acutely injured human cerebral cortex. *Brain* **129**, 778–790.
- Fatt P & Ginsborg BL (1958). The ionic requirements for the production of action potentials in crustacean muscle fibres. *J Physiol* **142**, 516–543.

- Fern R, Davis P, Waxman SG & Ransom BR (1998). Axon conduction and survival in CNS white matter during energy deprivation: a developmental study. *J Neurophysiol* **79**, 95–105.
- Fern R & Harrison PJ (1988). Conduction slowing and conduction block induced by high extracellular calcium concentration in isolated nerve fibres of the frog, *Rana temporaria*. *J Physiol* **406**, 108P.
- Fern R, Ransom BR & Waxman SG (1995). Voltage-gated calcium channels in CNS white matter: role in anoxic injury. *J Neurophysiol* **74**, 369–377.
- Fletcher CF & Frankel WN (1999). Ataxic mouse mutants and molecular mechanisms of absence epilepsy. *Hum Mol Genet* **8**, 1907–1912.
- Fletcher CF, Lutz CM, O'Sullivan TN, Shaughnessy JD Jr, Hawkes R, Frankel WN, Copeland NG & Jenkins NA (1996). Absence epilepsy in tottering mutant mice is associated with calcium channel defects. *Cell* **87**, 607–617.
- Fletcher CF, Tottene A, Lennon VA, Wilson SM, Dubel SJ, Paylor R, Hosford DA, Tessarollo L, McEnery MW, Pietrobon D, Copeland NG & Jenkins NA (2001). Dystonia and cerebellar atrophy in *Cacna1a* null mice lacking P/Q calcium channel activity. *FASEB J* **15**, 1288–1290.
- Forti L, Pouzat C & Llano I (2000). Action potential-evoked Ca^{2+} signals and calcium channels in axons of developing rat cerebellar interneurons. *J Physiol* **527**, 33–48.
- Foster RE, Connors BW & Waxman SG (1982). Rat optic nerve: electrophysiological, pharmacological and anatomical studies during development. *Brain Res* **255**, 371–386.
- Friedman S & Shatz CJ (1990). The effects of prenatal intracranial infusion of tetrodotoxin on naturally occurring retinal ganglion cell death and optic nerve ultrastructure. *Eur J Neurosci* **2**, 243–253.
- Gallo V & Ghiani CA (2000). Glutamate receptors in glia: new cells, new inputs and new functions. *Trends Pharmacol Sci* **21**, 252–258.
- Girault JA & Peles E (2002). Development of nodes of Ranvier. *Curr Opin Neurobiol* **12**, 476–485.
- Henley J & Poo MM (2004). Guiding neuronal growth cones using Ca^{2+} signals. *Trends Cell Biol* **14**, 320–330.
- Hildebrand C & Waxman SG (1984). Postnatal differentiation of rat optic nerve fibers: electron microscopic observations on the development of nodes of Ranvier and axoglial relations. *J Comp Neurol* **224**, 25–37.
- Hille B (1998). *Ionic Channels of Excitable Membranes*. Sinauer Associates, Sunderland, MA.
- Inchauspe CG, Martini FJ, Forsythe ID & Uchitel OD (2004). Functional compensation of P/Q by N-type channels blocks short-term plasticity at the calyx of held presynaptic terminal. *J Neurosci* **24**, 10379–10383.
- Ishibashi T, Dakin KA, Stevens B, Lee PR, Kozlov SV, Stewart CL & Fields RD (2006). Astrocytes promote myelination in response to electrical impulses. *Neuron* **49**, 823–832.
- Jenkins SM & Bennett V (2002). Developing nodes of Ranvier are defined by ankyrin-G clustering and are independent of paranodal axoglial adhesion. *Proc Natl Acad Sci U S A* **99**, 2303–2308.
- Jun K, Piedras-Renteria ES, Smith SM, Wheeler DB, Lee SB, Lee TG, Chin H, Adams ME, Scheller RH, Tsien RW & Shin HS (1999). Ablation of P/Q-type Ca^{2+} channel currents, altered synaptic transmission, and progressive ataxia in mice lacking the α_{1A} -subunit. *Proc Natl Acad Sci U S A* **96**, 15245–15250.
- Kaplan MR, Meyer-Franke A, Lambert S, Bennett V, Duncan ID, Levinson SR & Barres BA (1997). Induction of sodium channel clustering by oligodendrocytes. *Nature* **386**, 724–728.
- Kárádóttir R, Cavalier P, Bergersen LH & Attwell D (2005). NMDA receptors are expressed in oligodendrocytes and activated in ischaemia. *Nature* **438**, 1162–1166.
- Kolk SM, Nordquist R, Tuinhof R, Gagliardini L, Thompson B, Cools AR & Roubos EW (2000). Localization and physiological regulation of the exocytosis protein SNAP-25 in the brain and pituitary gland of *Xenopus laevis*. *J Neuroendocrinol* **12**, 694–706.
- Komada M & Soriano P (2002). β IV-spectrin regulates sodium channel clustering through ankyrin-G at axon initial segments and nodes of Ranvier. *J Cell Biol* **156**, 337–348.
- Konur S & Ghosh A (2005). Calcium signaling and the control of dendritic development. *Neuron* **46**, 401–405.
- Kukley M, Capetillo-Zarate E & Dietrich D (2007). Vesicular glutamate release from axons in white matter. *Nat Neurosci* **10**, 311–320.
- Lambert S, Davis JQ & Bennett V (1997). Morphogenesis of the node of Ranvier: co-clusters of ankyrin and ankyrin-binding integral proteins define early developmental intermediates. *J Neurosci* **17**, 7025–7036.
- Leppanen L & Stys PK (1997). Ion transport and membrane potential in CNS myelinated axons I. Normoxic conditions. *J Neurophysiol* **78**, 2086–2094.
- Lindsey JD & Ellisman MH (1985). The neuronal endomembrane system. III. The origins of the axoplasmic reticulum and discrete axonal cisternae at the axon hillock. *J Neurosci* **5**, 3135–3144.
- Lorenzon NM, Lutz CM, Frankel WN & Beam KG (1998). Altered calcium channel currents in Purkinje cells of the neurological mutant mouse leaner. *J Neurosci* **18**, 4482–4489.
- Mackenzie PJ, Umemiya M & Murphy TH (1996). Ca^{2+} imaging of CNS axons in culture indicates reliable coupling between single action potentials and distal functional release sites. *Neuron* **16**, 783–795.
- Meier H (1968). The neuropathology of ducky, a neurological mutation of the mouse. A pathological and preliminary histochemical study. *Acta Neuropathol (Berl)* **11**, 15–28.
- Meier H & MacPike AD (1971). Three syndromes produced by two mutant genes in the mouse. Clinical, pathological, and ultrastructural bases of tottering, leaner, and heterozygous mice. *J Hered* **62**, 297–302.
- Micu I, Jiang Q, Coderre E, Ridsdale A, Zhang L, Woulfe J, Yin X, Trapp BD, McRory JE, Rehak R, Zamponi GW, Wang W & Stys PK (2006). NMDA receptors mediate calcium accumulation in myelin during chemical ischaemia. *Nature* **439**, 988–992.

- Mintz IM, Venema VJ, Swiderek KM, Lee TD, Bean BP & Adams ME (1992). P-type calcium channels blocked by the spider toxin ω -Aga-IVA. *Nature* **355**, 827–829.
- Nakata T, Terada S & Hirokawa N (1998). Visualization of the dynamics of synaptic vesicle and plasma membrane proteins in living axons. *J Cell Biol* **140**, 659–674.
- Peters O, Schipke CG, Hashimoto Y & Kettenmann H (2003). Different mechanisms promote astrocyte Ca^{2+} waves and spreading depression in the mouse neocortex. *J Neurosci* **23**, 9888–9896.
- Rasband MN, Peles E, Trimmer JS, Levinson SR, Lux SE & Shrager P (1999). Dependence of nodal sodium channel clustering on paranodal axoglial contact in the developing CNS. *J Neurosci* **19**, 7516–7528.
- Rasband MN & Shrager P (2000). Ion channel sequestration in central nervous system axons. *J Physiol* **525**, 63–73.
- Rhyu IJ, Abbott LC, Walker DB & Sotelo C (1999a). An ultrastructural study of granule cell/Purkinje cell synapses in tottering (*tg/tg*), leaner (*tg^{la}/tg^{la}*) and compound heterozygous tottering/leaner (*tg/tg^{la}*) mice. *Neuroscience* **90**, 717–728.
- Rhyu IJ, Oda S, Uhm CS, Kim H, Suh YS & Abbott LC (1999b). Morphologic investigation of rolling mouse Nagoya (*tg^{rol}/tg^{rol}*) cerebellar Purkinje cells: an ataxic mutant, revisited. *Neurosci Lett* **266**, 49–52.
- Salter MG & Fern R (2005). NMDA receptors are expressed in developing oligodendrocyte processes and mediate injury. *Nature* **438**, 1167–1171.
- Salzer JL (2003). Polarized domains of myelinated axons. *Neuron* **40**, 297–318.
- Sanchez I, Hassinger L, Sihag RK, Cleveland DW, Mohan P & Nixon RA (2000). Local control of neurofilament accumulation during radial growth of myelinating axons in vivo. Selective role of site-specific phosphorylation. *J Cell Biol* **151**, 1013–1024.
- Shatz CJ (1996). Emergence of order in visual system development. *Proc Natl Acad Sci U S A* **93**, 602–608.
- Smith JM, Bradley DP, James MF & Huang CL (2006). Physiological studies of cortical spreading depression. *Biol Rev Camb Philos Soc* **81**, 457–481.
- Stevens B, Tanner S & Fields RD (1998). Control of myelination by specific patterns of neural impulses. *J Neurosci* **18**, 9303–9311.
- Stys PK, Waxman SG & Ransom BR (1992). Ionic mechanisms of anoxic injury in mammalian CNS white matter: role of Na^+ channels and Na^+ - Ca^{2+} exchanger. *J Neurosci* **12**, 430–439.
- Sun BB & Chiu SY (1999). N-type calcium channels and their regulation by GABAB receptors in axons of neonatal rat optic nerve. *J Neurosci* **19**, 5185–5194.
- Tait S, Gunn-Moore F, Collinson JM, Huang J, Lubetzki C, Pedraza L, Sherman DL, Colman DR & Brophy PJ (2000). An oligodendrocyte cell adhesion molecule at the site of assembly of the paranodal axo-glial junction. *J Cell Biol* **150**, 657–666.
- Thomas R, Salter MG, Wilke S, Husen A, Allcock N, Nivison M, Nnoli AN & Fern R (2004). Acute ischemic injury of astrocytes is mediated by Na-K-Cl cotransport and not Ca^{2+} influx at a key point in white matter development. *J Neuropathol Exp Neurol* **63**, 856–871.
- Wakamori M, Yamazaki K, Matsunodaira H, Teramoto T, Tanaka I, Niidome T, Sawada K, Nishizawa Y, Sekiguchi N, Mori E, Mori Y & Imoto K (1998). Single tottering mutations responsible for the neuropathic phenotype of the P-type calcium channel. *J Biol Chem* **273**, 34857–34867.
- Yang Y, Lacas-Gervais S, Morest DK, Solimena M & Rasband MN (2004). β IV spectrins are essential for membrane stability and the molecular organization of nodes of Ranvier. *J Neurosci* **24**, 7230–7240.
- Ziskin JL, Nishiyama A, Rubio M, Fukaya M & Bergles DE (2007). Vesicular release of glutamate from unmyelinated axons in white matter. *Nat Neurosci* **10**, 321–330.

Acknowledgements

This work was supported by the National Institutes of Neurological Disorders and Stroke grant NS 44875 to R.F. and an MRC programme grant to A.C.D. We wish to thank Dr Peles (Weizmann Institute of Science, Israel) for the generous gift of ant-CASPR-1 and Dr Komada (Tokyo Institute of Technology) for kindly providing anti- β IV spectrin. We acknowledge the excellent technical assistance of Natalie Allcock and Stuart Martin, and thank Abbie Fairs for her excellent electron microscopy work (Supplemental Fig. 4).

Supplemental material

Online supplemental material for this paper can be accessed at: <http://jpp.physoc.org/cgi/content/full/jphysiol.2008.155077/DC1>